Journal Pre-proofs

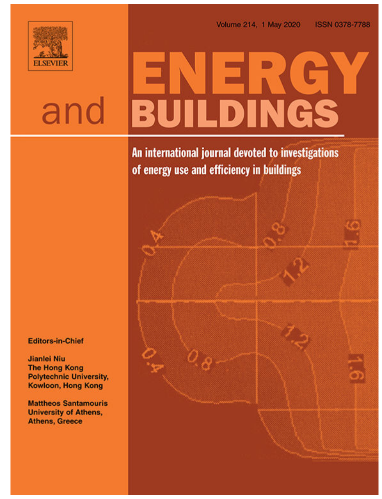

Heat exposure during a power outage: A simulation study of residences across the metro Phoenix area

Mayuri Rajput, Godfried Augenbroe, Brian Stone, Matei Georgescu, Ashley Broadbent, Scott Krayenhoff, Evan Mallen

PII: S0378-7788(21)00889-6
DOI: https://doi.org/10.1016/j.enbuild.2021.111605
Reference: ENB 111605

To appear in: *Energy & Buildings*

Received Date: 14 July 2021
Revised Date: 14 October 2021
Accepted Date: 19 October 2021

Please cite this article as: M. Rajput, G. Augenbroe, B. Stone, M. Georgescu, A. Broadbent, S. Krayenhoff, E. Mallen, Heat exposure during a power outage: A simulation study of residences across the metro Phoenix area, *Energy & Buildings* (2021), doi: https://doi.org/10.1016/j.enbuild.2021.111605

Heat exposure during a power outage: A simulation study of residences across the metro Phoenix area

Mayuri Rajput[1], Godfried Augenbroe[1], Brian Stone[1], Matei Georgescu[2], Ashley Broadbent[2],

Scott Krayenhoff[3], Evan Mallen[1]

[1]Georgia Institute of Technology

[2]Arizona State University, School of Geographical Sciences and Urban Planning

[3]University of Guelph, School of Environmental Sciences

Corresponding Author Details:
Mayuri Rajput
Email: Mayuri.rajput@gatech.edu
Address: 800 Peachtree Street NE, Apartment 8423, Atlanta, GA-30308
LinkedIn: www.linkedin.com/in/mayurir

Keywords: Climate change, resiliency, weather research and forecasting, thermal comfort, heat stress, urban simulation

Abstract

In the wake of growing concern for climate change, heat waves and their potential health effects (McGeehin & Mirabelli, 2001) have become a recurring phenomenon (Beniston, 2004; Fouillet et al., 2006). Extreme heat events in the USA are responsible for more deaths as compared to other weather events such as hurricanes, lightning, tornadoes and floods (Luber & McGeehin, 2008). Heat exposure in buildings has risen due to global warming in conjunction with other factors like urbanization and associated heat island effects (Kolokotroni, Ren, Davies, & Mavrogianni, 2012), lack of thermal mass (Lomas & Porritt, 2017a), exposure to solar insolation on higher stories, absence of window shading, overcrowding and envelope properties exacerbate the overheating inside the dwellings (Vellei et al., 2017). Stone et al. (2021) provides a macro view of the indoor environments in buildings due to the concurrent event of power outage during heat wave in face of climate change. This paper builds on the previous publication and provides a detailed view of modeling methodology, building physics that explains the sources/sinks of heat and entails a detailed evaluation of the current building stock for the low to moderate income residences in the city of Phoenix, Arizona in terms of their thermal performance. Finite Element models of building stock were simulated using MATLAB for microclimate weather files of Phoenix generated by Weather Research and Forecasting (WRF) simulation. Significant differences in temperature were noted in same building archetypes in different pockets of the city indicating the role of urbanization in aggravating the impact of heat wave. Dwellings with high thermal mass are found to be much more resilient to high ambient temperatures as compared to code compliant residences with basements being the coolest zones in all prototypes.

1 Introduction

After severe heatwaves of Europe in 2006 (Rebetez, Dupont, & Giroud, 2009) and New York in 2003 (Anderson & Bell, 2012), research in overheating of dwellings gained momentum with building simulation community trying to assess the performance of current housing stock in the event of heatwaves (Baniassadi, Heusinger, & Sailor, 2018; Lomas & Porritt, 2017b). The question of passive survivability in the context of code compliant buildings have led to multiple studies where buildings are subjected to extreme heat waves along-with the shock event of a power outage due to increased load on the electric grid. It came to the fore in these studies that temperate and cold climates can benefit from increased ventilation in such events (Hamdy, Carlucci, Hoes & Hensen, 2017) but for buildings that are located in cooling dominated regions such as tropics and sub-tropics, they must take additional measures such has high thermal mass, improved natural ventilation and high roof albedo to avoid overheating in air-tight and high insulation buildings (Baniassadi, Huesinger & Sailor, 2018). With untamed emissions, an increase of 1.5 degree C is all but inevitable and the heatwaves are expected to be more extreme with longer heat spells. This is exacerbated by Urban Heat Island (UHI) effect in cities with a large built-up area which was once covered with vegetation. The mineralization of urban areas not only traps heat but retains it for a long time due to material properties of roads, buildings, and pavements. Urban canyons resist the flow of wind that would otherwise flush out the heat by convective heat transfer mechanisms. Due to these factors, the weather has changed significantly both on temporal as well as spatial resolution with hyper localized weather in some parts of the cities as compared to others.

With the advent of numerical models for prediction of future weather, building simulation are coupled with weather simulation models for obtaining locale weather for urban energy simulations as well as modeling thermal response of buildings for different climate change scenarios (Ciancio et al., 2018; Falasca et al., 2019; Touchaei & Akbari, 2015). Just as building simulation computes the energy fluxes within the building and across the envelope of building, weather simulation models such as ENVI-MET (Bruse et al., 2004), UWG (Bueno, Norford, Hidalgo, & Pigeon, 2013), WRF (Skamarock et al., 2005) and TEB (Masson et al., 2002). compute the heat and hydrological fluxes for a geographical location to derive weather that is local to the site. The dynamic modeling of variation in wind requires specialized tools that works on the principles of Computational Fluid Dynamics (CFD) such as OpenFOAM, ANSYS Fluent or STAR-CCM (Liu et al., 2017) and can simulate the wind speed and pressure coefficients in an urban setting for use in building simulation. Coupling between building simulation and microclimate models is complex due to difference in temporal and spatial scales, computationally expensive due to exchange of data back and forth between two simulation environment and works best for handcrafted models of limited number of buildings for a geographical area not bigger than a neighborhood. They are particularly not suited for projects that span for larger areas or whole cities.

Problem Statement: This study demonstrates the vulnerability of existing houses in the city of Phoenix by forcing Building Energy Model with the output of Weather Research and Forecasting model to provide an insight into the thermal resilience of residential buildings and the impact of building codes on their comfort profile for current and future weather scenarios. EIA reports that one in three households in the US faced challenges to pay their energy bills (Berry et al., 2015) and 89% of the low income houses were found to be of inadequate quality (Lee et al., 2011) making them more vulnerable to overheating in the event of a heatwave. These houses have been represented in the study where cooling capacity of air conditioning system is not sufficient to condition the unit even if there is no power outage. The results are being used by urban planning experts to estimate the population that is at risk of extreme heat due to heatwaves and would be published once the analysis is complete.

A series of prototypes are created to represent the full range of residential living, i.e., single story residence, two-story residence and multi-family housing in Phoenix. For each of the prototypes a range of variants are considered, related to vintage, building style and code compliance per location and year of construction, structural composition of the envelope, presence of basement, and shading related to tree density on site. For the multifamily case, location variants such as most and least sun exposed variants are distinguished. Each of the prototype variants is subjected to a simulation scenario consisting of a period of regular usage with functioning HVAC (9 days), followed by five days of heatwave during which a complete power outage occurs. A dynamic simulation model is used to predict the temperatures during the power outage, in the various living spaces and basement followed by eight days of "recovery" period. During the recovery the building is cooled down until the normal daily temperature regime is reached. The neighborhood climate during the simulation is available from localized Weather Research and Forecasting (WRF; Chen et al. 2011; Skamarock et al. 2005; see section 2.4) regional climate simulations for contemporary as well as mid and late 21st century periods. Aggressive mitigation strategies to reduce urban heat island effect have also been simulated by the WRF model where hypothetical scenarios of near 100% adaptation of cool roofs and increased vegetation in city are modeled for maximum potential cooling by trees. In running the batch of building simulations, the effect of several operational variables are considered, mainly related to the opening of windows to ventilate with outside air whenever this alleviates the thermal discomfort inside.

The outcomes of the simulations are presented as temperature exposure during different time periods in the 21st century, across the city of Phoenix and in different building prototypes with mitigation strategies mentioned in previous paragraph.

2. Methodology

2.1 Building Archetypes

Assessment of the current building stock may be done through surveys as well as databases offered by government bodies specializing in city and regional planning. Studies such as (Augenbroe et al., 2008; Lim & Zhai, 2017; Zhao, Lee, & Augenbroe, 2016) represent ways in which archetypical buildings act as representatives of a city's building stock for energy as well as comfort assessments. To generate the prototypes of residential buildings in the city of Phoenix, we use the generic residential prototypes published by US DOE, Building Energy Codes Program as the baseline for our approach. Some prototypes are in fact offered as thermal simulation models in the EnergyPlus (PNNL, 2013) input format. For the purpose of our study, these EnergyPlus input models are reverse-engineered to find all relevant construction information about geometry, window type and locations and materials used in construction. Some inconsistencies in the specification of building such as presence of very small overhangs on windows are remodeled during this step.

The following lists the prototypes that are used as baseline for the study:

1. Single Family detached house (Figure 1)
    a. Single story house without basement
    b. Two story house with basement
    c. Two story house without basement

2. Multi Family apartment building
    a. Apartment facing Southeast corner of building on the top floor
    b. Apartment facing North direction with apartments on all sides

Although there are a total of 18 units in the multi-family homes, two cases representing maximum and minimum contact (depending on sun exposure and building envelope exposure) to the external boundary conditions are considered. The unit on the North face of the building receives minimum solar irradiation owing to just one wall receiving mostly diffuse solar irradiance. In addition to this low exposure to the outside climate the ground floor apartment is situated above the concrete floor slab and adjoining soil which provides it access to a relatively large active thermal mass.

On the other hand, South-East and South-West top corner units not only receive both direct and diffuse solar irradiance on two walls but are also directly connected to a large roof facing South at an inclination of 62.5°.As a result, these two units (North facing and South-east corner) would represent the two extremes between which all other apartment thermal responses can be estimated.

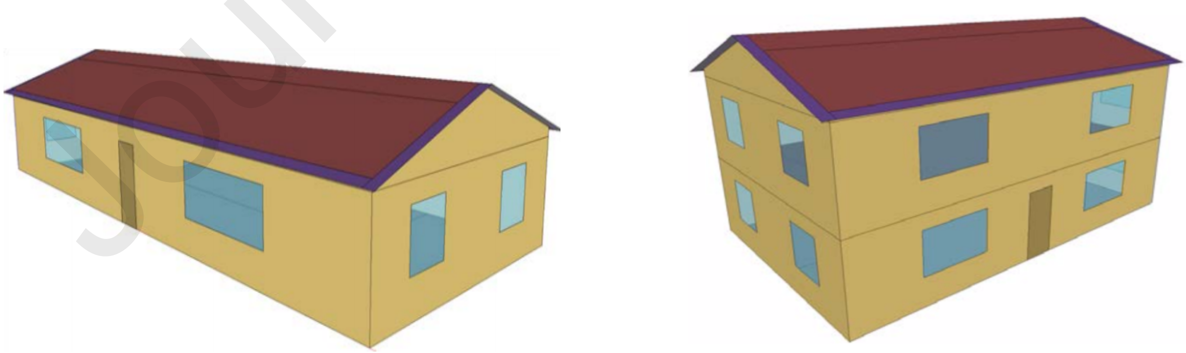

Figure 1. Single Family detached houses

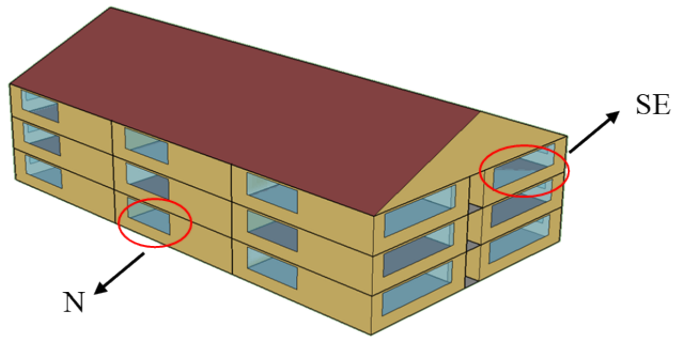

Figure 2. Multi-family housing

The foundation for all prototypes without basement is slab on grade. Multi-family prototypes further have two construction variants namely IECC 2006 and IECC 2012.

Detached single family residences have constructions conforming to codes *IECC 2006* and *High Thermal Mass enclosures*. As the name suggests, high thermal mass enclosures represent the family of buildings with exterior walls consisting of high density materials (of the likes of double brick or concrete block) with an insulation layer in direct vicinity of indoor space. With the exception of single family single story residences that represent the older most dilapidated structures of the housing repository, each prototype meets strict insulation requirements between attic and living areas of house. The details of construction properties of each of the vintages are provided in the Appendix section.

Arizona being a home rule state, mandatory building energy codes are adopted and enforced on a local level. The movement to encourage building energy efficiency started in 1999 with the formation of the Joint Legislative Energy Efficiency Code Study Committee. The committee led to enactment of Housing bill 2322 which required state agencies to adopt energy efficiency measures.

The report generated by PNNL in 2012 (Cort & Butner, 2012) apprise that at least 87% of all the residential buildings conform to IECC 2006 or above. A DOE study claims that approximately 65% of all new construction in the state conforms to IECC 2012 building code (Building energy Codes Program , 2011).

2.2 Sub-variants of the archetypical residences

For every residence variant the following sub-variants are introduced, related to the way the occupants operate their residence (in normal use and during the outage), the maintenance state of their HVAC equipment, and the presence and density of nearby trees.

2.2.1 Orientation

In a city with known building stock, the orientation of the buildings is to a large extent random, although in some climate zones a certain orientation may be dominant based on cultural preferences. It is important to verify whether the orientation of the prototypes has a large influence on the outcomes. To assess the extent to which orientation plays a role in the temperature profile of building zones, one prototype (single family single story) was simulated for all cardinal directions. We assume for the single residences that all walls are exposed to solar irradiation.

As each side is not significantly different in size, WWR and U-values being same on each side and with no (external) shading provisions, it may be concluded from Figure 3 that orientation does not play a significant role in the considered building prototypes in a power outage scenario.

Similar results were observed for the two-story residence. Based on these results it is decided to conduct all simulations for one fixed orientation.

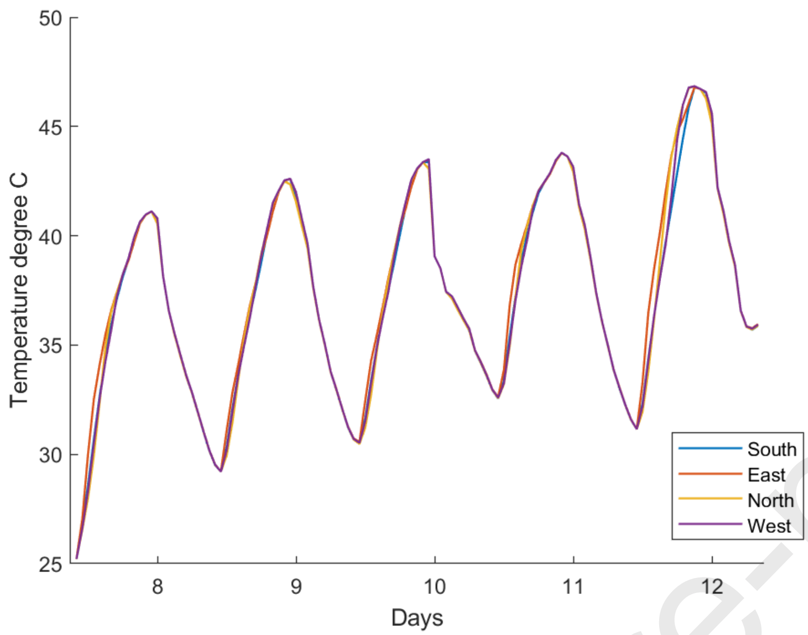

Figure 3 Effect of orientation on temperature in a free floating(unconditioned) single family, single story house

2.2.2 Shading by Trees

2.2.2.1 Effect of shading by trees

The planting of trees that are close enough to the residence to provide shading is often used to reduce the cooling load (Wang, Zhao, Yang, & Song, 2016) and glare in the buildings. The presence of trees reduces surface temperature of facades by radiative shading (direct blocking of solar radiation) with reported reduction of up-to 30% cooling in HVAC loads (Akbari, Kurn, Bretz, & Hanford, 1997). In our study we are interested to include the effect of different tree arrangements on the resulting temperatures in the residence. The secondary effect of reduced wind speed and cooling due to evapotranspiration has not been included in this study. It should be noted however that the much larger effect of urban vegetation at the larger scale is accounted for in the urban weather predictions used in this study, as will be reported later. The effect of the trees in the immediate vicinity of the residences is therefore only accounted in the amount of blockage of solar irradiation on facades, windows, and roof.

For cities in arid or semi-arid environment such as Phoenix, shade trees and urban lawns are the two popular forms of urban vegetation; shade trees are usually presented in xeric landscapes with parsimonious irrigation requirement, while urban lawns are commonly found in mesic landscape with ample irrigation.

2.2.2.2 Variance in properties of trees

A literature review was used to characterize the most common the type of vegetation found in the Southwest in so far as it acts as shading trees in xeric (desert) landscape. The blockage of solar insolation due to shading trees depend on the following properties of tress, namely;

Crown Density: Transmissivity of solar radiation depends on the crown density and opacity of leaves. The crown density of tree varies with specie and foliation period. However, in summer season the variation on the crown density of all dominant species in the Southwest is approximately 10% (McPherson & Dougherty, 1989) hence the study takes a constant value for crown density.

Tree Size and age: The variation in full growth height amongst various species of tree in Phoenix range between 5 feet and 17 feet (Adkins, n.d.). Height in combination with crown density and bole height result in considerable permutations of tree arrangements around a residential building.

Effect of direction and distance from house: Tree to building distance of 2m to 5m are commonly considered in shading studies structure (Hwang, Wiseman, & Thomas, 2015) as there is very little information about general tree location relative to building facades. In addition to distance, direction plays an important role in radiative shading as in the Northern hemisphere, shading on a South façade results in lower heat gain by the built form (Simpson, 2002) and vise-versa for the Southern hemisphere

There can be countless possibilities in tree species and arrangements around a residential building. For our study we are only interested in the maximum shading that can be reasonably obtained in Phoenix. This will serve as one end of the shading spectrum whereas the other extreme is no trees at all. By simulating both extremes, this approach provides a means to interpolate between the no-shading and best shading scenarios of the building prototypes. To calculate the maximum shading potential, Palo-verde with a height of 7 meters (age- 5 years) has been assumed to be placed in four cardinal directions around the house. Calculation of shading factors and their use in the simulation model will be described later.

2.2.3 Airflow Network

Any outside air entering the built form acts as an additional heating or cooling load on the living spaces of the building. The amount of air exchange with the environment depends on multiple factors such as building geometry (affecting wind pressure coefficients on each surface), presence of wind canyons around building, obstructions (trees and other buildings), wind speed and direction and temperature differential between the zone behind a façade opening and the environment. Facade openings can be either controlled (occupant-controlled windows and doors) or uncontrolled. The first leads to controlled natural ventilation, the latter occurs as uncontrolled ventilation or air infiltration.

2.2.3.1 Variation in air exchange

Infiltration: Infiltration is the adventitious flow of air from the outdoor environment via openings such as cracks around windows, opening and closing of doors and sometimes through poorly sealed elements and joints of the building fabric and principally at edges around windows and doors.

Air exchange is the airflow between outside and inside and between thermal zones inside the building. This cross-zone air flow passes through internal doors and other openings due to temperature and pressure differences across zones. An average ACH of 0.7 is assumed in this study for inter-zone air mixing. There is however no air exchange assumed between attic and conditioned zones of the building in line with strict code requirements.

Table 1 illustrates the Building Energy Codes Air Leakage guide (Building energy Codes Program , 2011) recommendations for residential constructions considered in this study and the assumptions that have been followed in modeling them based on ASHRAE Handbook-Fundamentals, 2017 and (Chan,Nazaroff, Price, Sohn & Gadgil, 2005).

Table 1. Infiltration through external enclosure for Building Prototypes

Building Code	IECC 2006	IECC 2009	IECC 2012
Air Change Rate (requirement)	No requirement	<7@50Pa	<3@50Pa
Assumed ACH in simulation model	2.5	1.5	1

Ventilation: Ventilation in a residential building may be of two types, namely, mechanical ventilation and natural ventilation.

Mechanical ventilation is the designed inflow of air in dwellings to refresh indoor air and preserve healthy indoor environment quality for its occupants. In the past, no specific requirements for ventilation were imposed for residential buildings because leakage through the envelope combined with controlled natural ventilation were considered adequate to maintain sufficient indoor air quality.

As envelope construction practices improved, the need to provide fresh air to homes via mechanical means has increased. Both IRC 2012 (International Residential Code) and IECC 2012 mandate that for buildings with infiltration of less than 5 ACH[1], a whole house mechanical ventilation is mandatory. Mechanical ventilation of 1 ACH has been assumed for all air conditioners simulated in this study in accordance with IRC 2012 recommendations.

Natural ventilation is the exchange of air with the outdoor environment through controllable openings solely driven by natural forces like wind pressure and stack effect driven by buoyancy. As discussed in (Djongyang, Tchinda, & Njomo, 2010; Jeong, Jeong, & Park, 2016), occupant behavior takes a dominant role in controlling the thermal environment inside the building when conditions are uncomfortable and occupants can control openings like windows for natural ventilation.

Single-sided volumetric air flow rate through openings is determined by equation 37 in Chapter 16 of ASHRAE fundamentals 2017 (American Society of Heating, Refrigerating and Air-Conditioning Engineers, 2017);

$$Q = C_v A_{opening} F_{schedule} V \tag{1}$$

[1] ACH= Number of air changes per hour

Where Q=Volumetric Flow rate driven by wind

C_v= Opening effectiveness (dimensionless)

$A_{opening}$=Opening area (m^2)

$F_{schedule}$= Open area fraction (dimensionless)

V=Local wind speed (m/s)

When the windows are open, it is assumed that the open area fraction is 1.0, i.e. totally open. This stems from the logic that an occupant will typically open the window when indoor air temperatures rise above the ambient temperature. Once the window is open it will rarely happen that outside temperature will be higher than the inside temperature, in which case we assume that the occupant will close the window. There are two phenomena that can cause this: (1) the living spaces are in contact with a significant amount of active thermal mass that may provide a form of cooling that leads to a decrease in room temperature, especially when there are no heat sources in the space; (2) there is significant long wave radiation loss to the nightly sky. Both phenomena provide a cooling effect. They are less likely to happen at night as Phoenix usually has large diurnal swings and the night temperatures typically reach such levels that night cooling with permanently open windows is the most likely scenario. Notwithstanding this, the simulations will be conducted with an embedded window opening control logic that will always find the most optimal control action.

2.2.4 HVAC Efficiency

For this study, zonal air conditioning controls are considered for each thermal zone in a way that they operate independent of each other. The unit supplies conditioned air at 18°C with a humidity ratio of 0.008kg/kg. The mass flow of air from the unit is constant during its operation.

2.2.4.1 Load calculations and extent of deficiency

Sensible load calculations are performed in accordance with American National Standards Institute (ANSI) recognized ACCA's updated ANSI/ACCA 2 Manual J – 2016 (Residential Load Calculations) (Rutkowski). Summer design day temperature for Phoenix is 43°C according to Table 1A of the manual and design indoor air temperature is 24°C. It should be noted that these calculations are performed for a typical design day and do not consider rare natural calamities like heat waves. Summer dehumidification or latent loads are ignored in this study as for an arid climate like Phoenix, there may be no condensate on the condensate coil and hence negligible latent load.

HVAC Deficiency: The degradation/deficiency in performance of residential air conditioners may happen due to many reasons such as undersized system, low air-flow, infiltration due to aged building and undercharged gas levels ("Monitored in-situ performance of residential air-conditioning systems / Discussion - ProQuest," n.d.). Three levels of efficiency -- 100%, 50% and 0% of (calculated) sensible load are simulated for all zones of mentioned building prototypes and their variants.

2.3 Thermal modeling approach

The first modeling phase consisted of extending and modifying the available EnergyPlus models (National Energy and cost savings for new single and multifamily homes- A comparison of 2006,2009 and 2012 editions of IECC) for the different subvariants and packaging them in a batch run that simulates all variants.

However, considering the large number of runs required for the whole city being represented by 1,800 weather files, Finite Element Modeling approach was preferred to increase the robustness using parallelization of available computing resources.

The prototypes are built using a standard finite element spatial discretization technique as discussed in (Augenbroe et al., 2008). It discretizes the building fabric and internal zones as a mesh of nodes and elements where the nodes represent state variables (temperatures) and the elements represent modes of heat transfer (conduction, convection, radiation and airflow).

A zone node represents the temperature of total mass of air contained in the room which is assumed to be well mixed and therefore uniform in temperature. Elements are the connection between nodes and their properties reflect the heat transfer mechanism operating between the respective nodes of the element.

Type of Element	**Connection**	**Physical factors affecting element**
Conduction		Thermal conductivity (W/m^2 K), Heat transfer area of nodes (m^2), thickness of element (m)
Convection		Convective heat coefficient h_c (W/m^2 K),Heat transfer area of nodes (m^2)
Radiation		Linearized radiative heat transfer coefficient h_{rad} (W/m^2 K), View factor (dimensionless), Heat transfer area of nodes (m^2)
Airflow		Wind velocity (m/s), Area of opening (m^2), schedule (dimensionless)
Type of Nodes	**Symbol**	**Property**
Air Node		Connection with other room surfaces via convective and radiative elements
Exterior Surface Node		Connected via conduction to inner layers and by convection and radiation to outer layers. Exposed to solar radiation.
Interior Surface Node		Connected to air node by conduction and radiation. Internal nodes are connected by conduction element
Interior Node		Connected by conduction element to other interior nodes and surface nodes
Prescribed nodes		Nodes that are not affected by all other nodes and are only dependent on weather conditions

Figure 4 Types and properties of nodes and elements

Several custom type elements can be used to increase the flexibility of the mesh generation, i.e. a so-called “Room-element” represents all transfer mechanisms in a room, whereas a “ventilation-element” is used to construct an airflow network between outside and inside and between internal zones. Boundary conditions at the external surfaces are modeled as elements that connect the nodes for ambient, sky and ground temperature to the surface node.

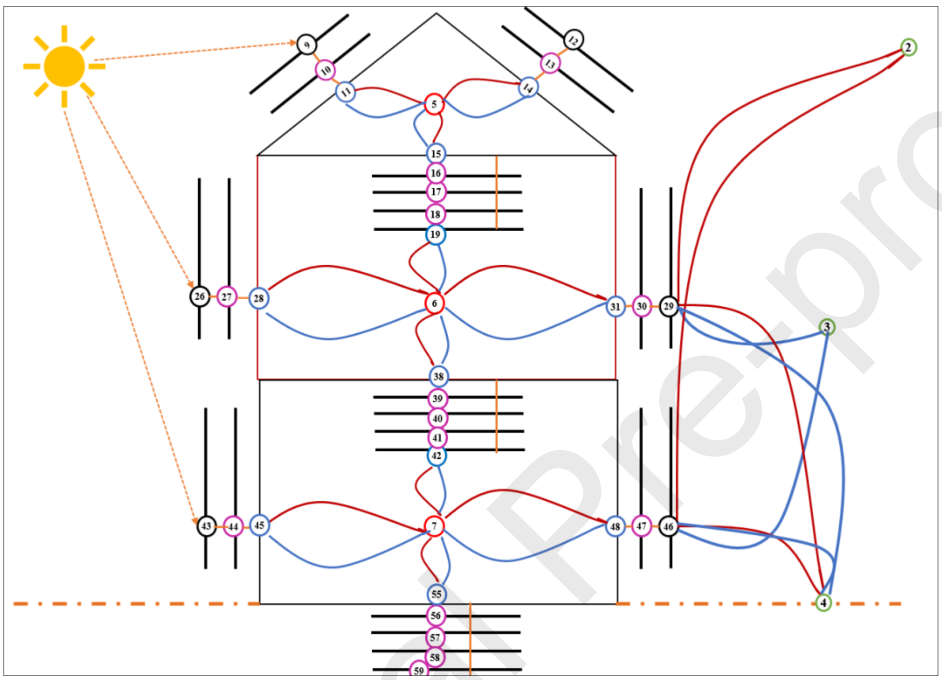

Figure 5 Nodal mesh diagram for MATLAB model

Using the standard finite element operation on the complete set of elements leads to the following differential algebraic equation (DAE) set:

$$M(t)\frac{dT}{dt} + S(T;t) = f(t) \qquad (2)$$

Where,

M(t)=Mass matrix (heat storage capacity)

S(T, t)= Stiffness matrix (heat exchange relationships)

f(t)= Load vector (thermal load on the nodes)

The load vector comprises of solar loads and metabolic heat gain by occupants of the thermal zone. Solar heat gain over a surface is calculated as

$$\dot{Q}_{sol,i} = F_{shad,i} A_i \varepsilon_i \dot{q}_{sol,i} \tag{3}$$

Where,

$F_{shad,i}$=Shading coefficient for surface I (dimensionless)

A_i= Area of exposed surface (m^2)

ε_i= Absorptivity of coating on surface I (dimensionless)

$\dot{q}_{sol,i}$= solar insolation incident on surface i (W/m^2)

Solar radiation incident on the exposed surfaces like wall and roof are calculated by a subroutine which uses equations presented in Chapter 14, section 2 of ASHRAE handbook. Incident solar radiation per unit area ($q_{sol,i}$)is computed and returned to the main program where it is multiplied by the area and shading coefficient of the surface to obtain solar thermal loads. **Error! Reference source not found.**6 illustrates the process for calculation of solar loads in formation of load vector f(t).

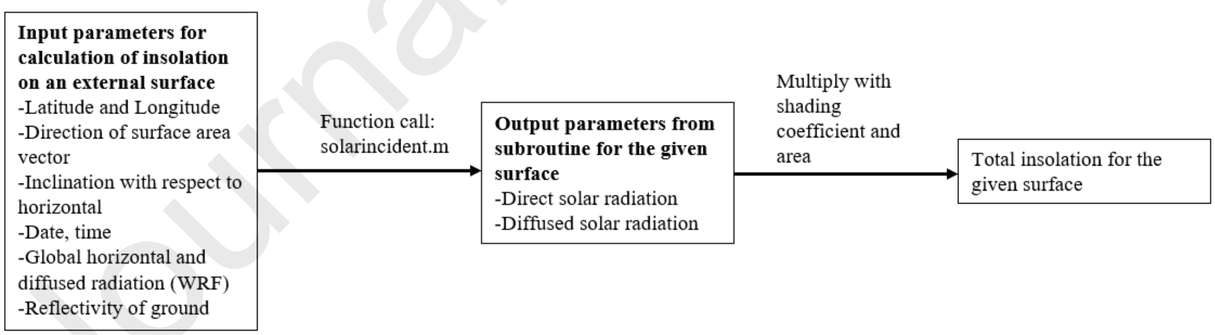

Figure 6 Computation of solar loads on each surface

Insolation falling on the windows make their way inside the dwelling either by conduction through window material or is directly transmitted inside the zone where window is mounted. Directly transmitted radiation is absorbed partly by mass present inside the room like furniture/ground and partly by air node. Transmission inside building as well as absorption of heat by window materials is governed by window properties which are recommended by the governing building codes.

Table 2 presents the residential building form requirements of IECC for Phoenix (Maricopa county, climate zone 2b);

Table 2. IECC building codes for building prototypes

Climate zone	IECC	Ceiling (R-value, °F·ft2·h/BTU)	Skylight (U-factor, Btu/hr · ft² · °F)	Fenestration (Windows and Doors)		Wood Frame Wall (R-value, °F·ft²·h/BTU)	Mass wall* (R-value,°F·ft2·h/BTU)	Floor (R-value, °F·ft²·h/BTU)	Basement wall* (R-value, °F·ft²·h/BTU)	Tested Max Air Leakage Rate (ACH)	Slab *** (R-value and depth)	Crawl Space** (R-value)
				U-factor (Btu/hr · ft² · °F)	SHGC							
2	2006	30	0.75	0.75	0.4	13	4/6	13	NR	NR	NR	NR
	2009	30	0.75	0.65	0.3					NR		
	2012	38	0.65	0.4	0.25					5		
*	The second number applies when more than half the insulation is on the interior side of the high mass material in the wall											
**	The first number is for continuous insulation (e.g., a board or blanket directly on the foundation wall) and the second number is for cavity insulation (i.e., if there is a furred-out wall built against the foundation wall). Only one of these two has to be met											
***	The first number is R-value. The second value refers to the vertical depth of the insulation around the perimeter											
NR	Not Required											

2.3.1 Usage scenarios

2.3.1.1 Batch control of simulation runs

As explained earlier, a variant simulation is run for a total of 22 days (9 pre-outage, 5 outage and 8 post outage days). A single warm up simulation cycle of three full years is performed to obtain the initial temperatures of all the nodes for each prototype with TMY3 data. Warm up ensures that temperature of all surfaces are at an equilibrium before the core simulation starts. Warm up stops at the date and time when the period of heat-wave starts.

Beyond this timestep, iteration for each WRF grid takes over the weather control and each prototype is simulated for the microclimate of that grid. Initial temperatures are reset to end of warm-up period at the start of each grid iteration.

Error! Reference source not found.7 shows the flowchart for the algorithm in which batch processing is performed for all the grid cell of Phoenix metro area. As an example, the heat-wave period starts on July 11 at 00:00 hours and ends on July 30, 00:00 hours.

Three years preceding to the start date -- July 10, 2003 – the system performs the warm up for all prototypes and stops at July 10, 2006 at 00:00 hours. This time stamp onwards, the environmental boundary conditions are switched from TMY to WRF data. The simulation is then performed with WRF data for 22 days. As the heat-wave period ends on July 30, 2006 at 00:00 hours, control moves back to initial temperatures of July 10,2006 at 00:00 hours with new set of WRF data-points for next grid cell.

This process is repeated for all the grids of Phoenix metro area and hourly temperature for all prototypes, and their variants are obtained for 528 hours (22 days*24).

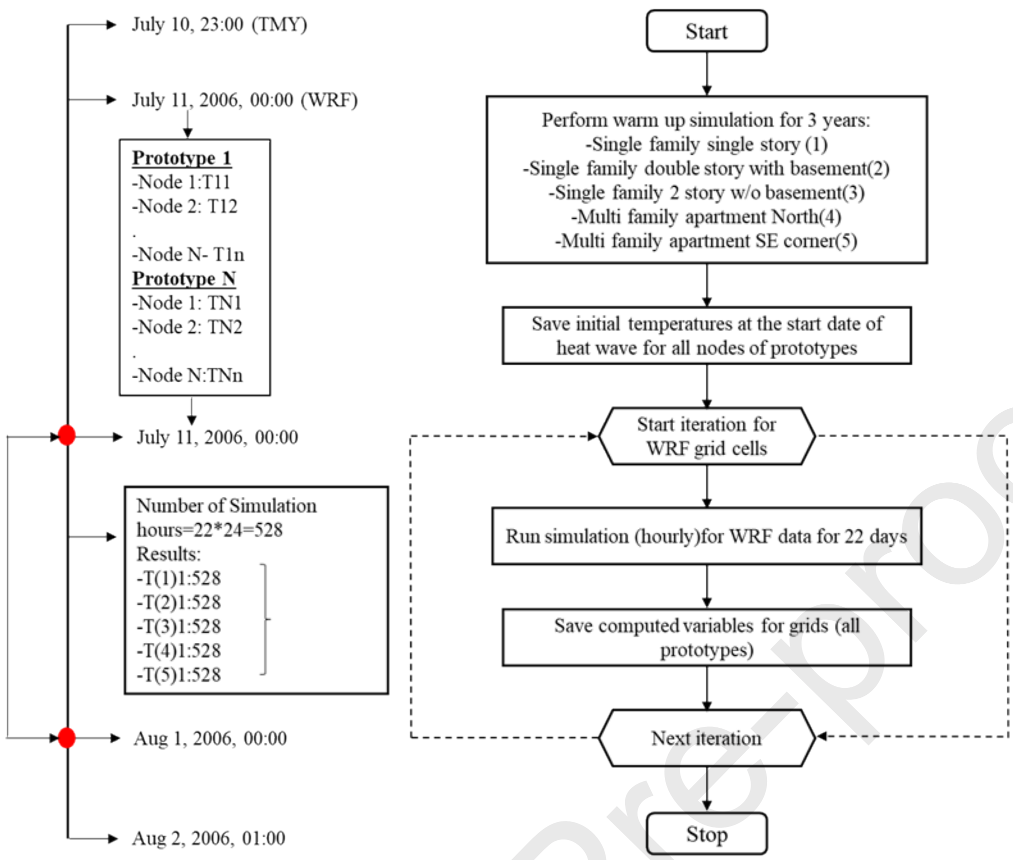

Figure 7 Flowchart for batch simulation of each variant of all building archetypes

2.3.1.2 Simulation scenario for heat-wave period

Heat-wave period has three distinct operating scenarios namely, pre-power outage, power outage and post power outage. Pre-power outage run ensures that the building is exposed to extreme heat on its skin while the interiors are being cooled by the air conditioner (with different variants of efficiency as discussed in section 2.2.4). Windows remain closed during this time and the airflow is due to infiltration only as discussed in section 2.2.3. This infiltration is modeled as a constant and depends on the vintage (construction code) of house in question.

During power outage, HVAC system and other devices such as fans are unavailable and there is no access to mechanical cooling. Occupant control is modeled by ventilation through opening of all windows of the room on a condition that the indoor temperature exceeds ambient temperature. When all windows are fully open, the ventilation rate is determined by the single side ventilation formula discussed in section 2.2.3.1.

2.3.1.3 Weather scenario

The WRF data consists of 1,800 grid cells with varying weather conditions depending on the topography and land use of the grid. The grids are sized with length and breadth of 1kmx1km and span from latitude [32.7888 to 34.1832] and longitudes [-112.9150 to -111.2854]. Grid cells with an urban fraction of 20% or more are chosen to be simulated for the indoor thermal conditions.

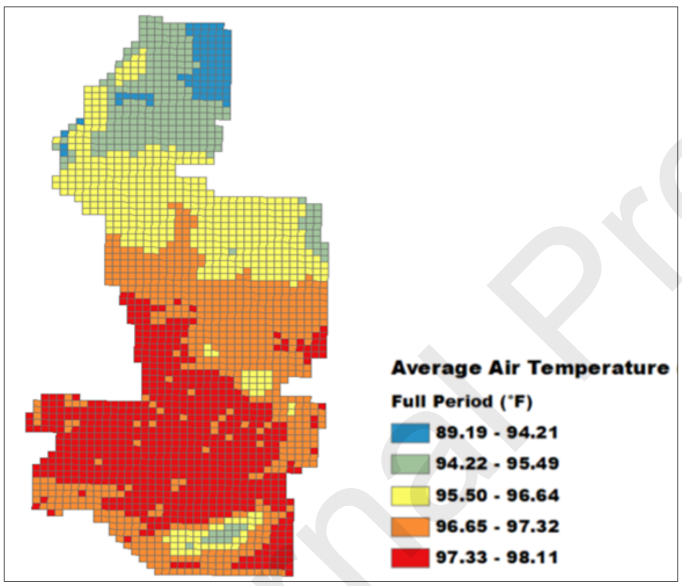

Figure 8 Weather grids in Phoenix (Mallen, 2019)

Data is received in NetCDF file format for each grid cell with 22 (days)* 24 data points for the following weather variables:

Table 3. Weather variables and their role in DAE

Variable	Unit	Comment
Ambient Temperature	º Celsius	Boundary condition for exterior surface nodes, Air flow network
Specific Humidity	kg/kg	Moisture balance model, Indoor Environment Quality, Heat Stress Indices
Direct Normal solar radiation	W/m^2	Solar loads on exposed surfaces (f matrix), Heat ingress in built space (solar load on air node)
Diffused solar radiation	W/m^2	Solar loads on exposed surfaces (f matrix), Heat ingress in built space (solar load on air node)
Wind speed (u)	m/s	Airflow network (Ventilation air change rate calculation)
Latitude		Representation of cumulative heat stress indices over a grid with centroid at a [latitude, longitude]
Longitude		

Error! Reference source not found. shows spatial and temporal variability of weather, based on detailed WRF simulations.

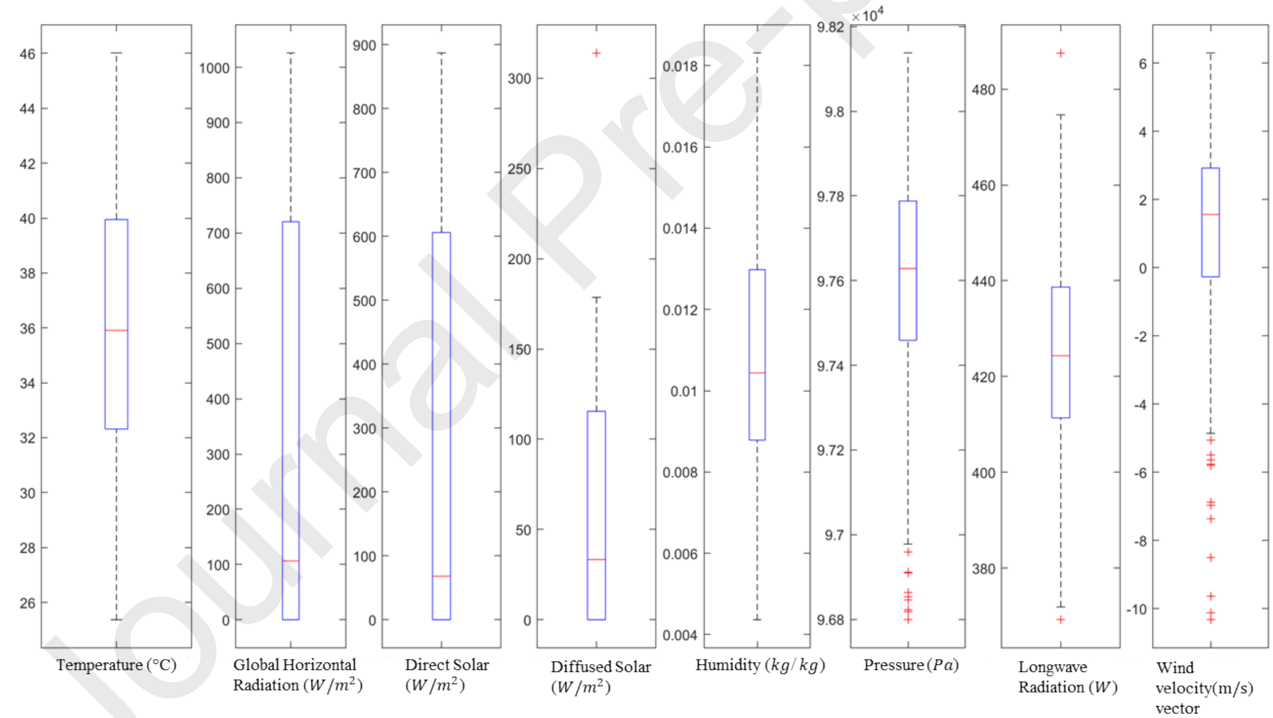

Figure 9 Variation in weather data across all grids of WRF

2.4 Weather Simulations for Forecasting

Five day heatwaves were simulated in Phoenix for the start mid-century and end of 21st century using the urbanized WRF mesoscale model. The WRF simulations made use of a multi-layer urban canopy model called the Building Environment Parametrization (BEP) (Martilli, Clappier, & Rotach, 2002), which is able to capture meteorological fields at street level between buildings. High-resolution, nested (1 km resolution for the innermost domain) two-way coupled WRF simulations allow the downscaling of the synoptic flow to the 1 km inner grid across the Phoenix metropolitan area. The Integrated Climate and Land Use Scenarios (ICLUS) dataset (Bierwagen et al., 2010) from the US Environmental Protection Agency for the continental US was applied to represent the evolving urban land cover and urban density over the 21st century. ICLUS urban classes range from rural/exurban, to medium intensity, and to high-intensity/commercial development, and they are integrated in the WRF domain using a method similar to a recent set of contiguous US climate simulations of urban expansion impacts (Krayenhoff, Moustaoui, Broadbent, Gupta, & Georgescu, 2018). A description of the WRF model setup and associated input datasets used in this study are found in (Broadbent, Krayenhoff, & Georgescu, 2020). Heat waves were identified as periods of five or more consecutive days where the 97.5th percentile daily average air temperature over the period 1980–2009 was exceeded. This approach to heat wave selection resulted in 10 such events, each with duration of at least 120 h) since 1980 for the Phoenix metropolitan area. The most intense of these heat wave events, occurring \July 18–25, 2006, was selected to drive the building energy simulations discussed herein. We simulated cool roofs with WRF by increasing the roof surface albedo of all rooftops to 0.88 from 0.16. We simulated provision of shading by trees and assumed that all intercepted solar radiation was converted to transpiration. This assumption provides an estimate of the maximum potential tree cooling. Trees were 10 m tall, covering approximately 50% of the between building space with an average leaf area index in the canyon space of 1.0 m^2 m^{-2}. Trees intercepted direct solar radiation according to Beer's law, assuming a spherical leaf angle distribution and scattering of 50% of solar radiation incident on leaves. This general approach to the attenuation of solar radiation by trees is detailed further in Huang et al. (2021), and it is a simplification of the BEP-Tree model ((Broadbent, Krayenhoff, & Georgescu, 2020); Krayenhoff et al., 2014)

Simulations were conducted in parallel on the high-performance computing clusters at Arizona State University. We utilized 112 processors for each simulation, with each experiment taking 48 hours to complete (approximately 5376 core hours). In total 36 simulations were conducted including base case, future climate, and adaptation scenarios. Each WRF simulation produced approximately 200 GBs of data, which equates to a total of 7.2 Terabytes of WRF-output data produced.

2.5 Special modeling features

2.5.1 Basement Model:

The basement of a building is the only thermal zone which is not directly exposed to solar irradiation and environmental boundary conditions. It is connected by convective heat transfer elements with the above grade thermal zone as well as with conductive heat transfer elements to soil surrounding the basement walls and floor. The connection between basement wall and ground exposed to ambient is done via pathways through soil.

ASHRAE (2003) provides a mathematical formulation where the amount of heat transferred through the soil (in the form of heat flow paths) is proportional to the depth of the basement construction, the difference between the external and internal temperatures, and on the type of the building. Floor portion adjacent to basement walls connect to the surface of earth through path length which has a fictitious depth of 1.5 times the depth of actual wall.

The path length is referenced from ASHRAE and represented in Table 5.

Table 4. Path lengths of nodes through soil in development of FEM model

Depth m	**Path Length Through soil m**
0.15	0.21
0.46	0.69
0.76	1.18
1.07	1.68
1.37	2.15
1.68	2.64
1.98	3.13

From that a fairly good linear regression (with R2= 0.9999) is:

Path length in soil= $-0.0352 + 1.5975 \times$ Depth

Path lengths for the basement are a surrogate for mass that dampens out any large fluctuations to the boundary conditions such as ambient temperature or solar insolation that may affect the air node of basement. Longer the path length, higher the active mass in-between air node and ground surface and hence higher the damping coefficient.

The model for unconditioned basement has been simulated and validated on Energy Plus in the initial phase of the project with a three day power outage as shown in Figure 10. The results from Finite Element Method agree well with the temperature profiles modeled by using Energy Plus.

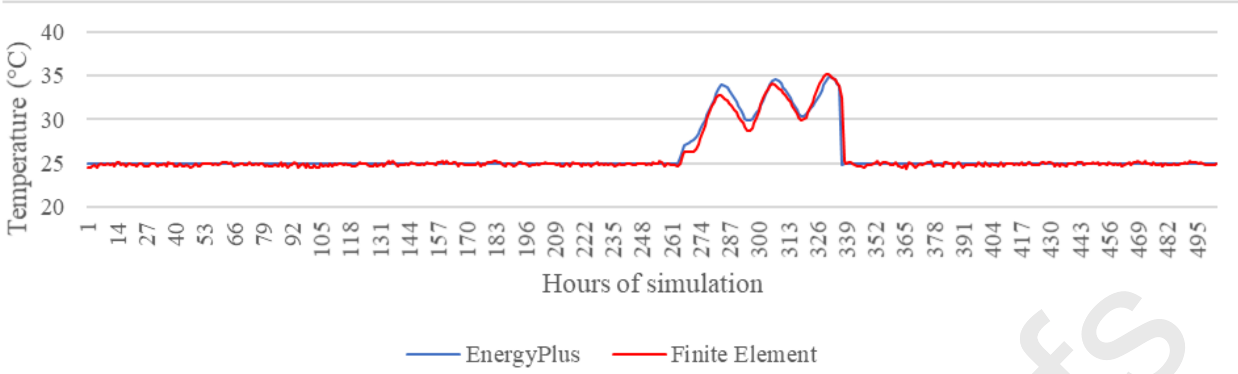

Figure 10 Comparison between temperature profiles from Energy Plus and Finite Element Method for basement

2.5.1.1 Finite Element Model for Basement

Figure 11 shows the dressed down version of the otherwise densely packed nodal model of basement and its interaction with other thermal zones as well as ambient weather conditions.

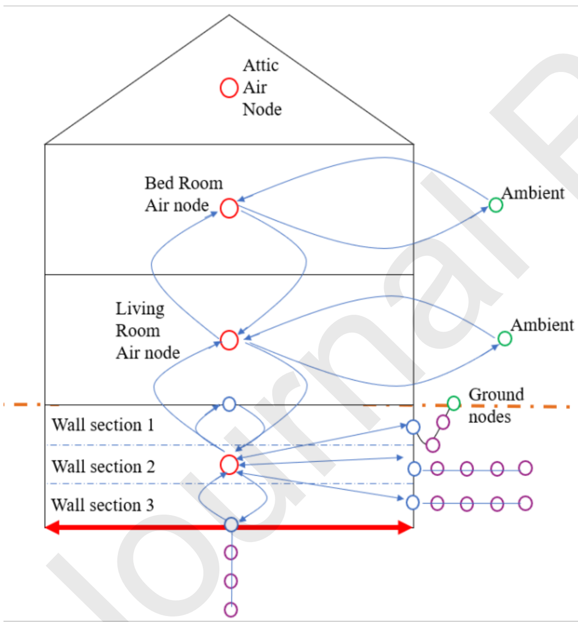

Figure 11 Basement air node heat transfer interactions

Each node along the path length is encased by a fictitious cuboid of active mass. Following example shows the methodology of calculating mass assignment to the nodes.

For wall section 1, there are four nodes that connect wall surface to ground nodes. The wedge formed between section 1 is a right-angled triangle with known depth and path length. Extent of influence for active mass contained in this wedge (assumed for simplicity of calculation) from building is calculated by Pythagoras theorem (see **Error! Reference source not found.**1).

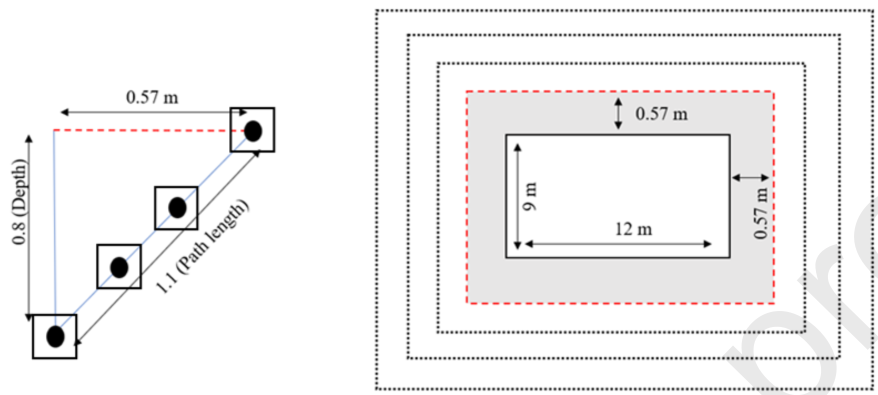

Figure 12 Calculation of active mass for each node

Area for this rectangle along the perimeter is;

A= (9+(0.57*2)) *0.57*2+12*0.57*2~25m^2

Area for each node =20/4=6.3 m^2

Thickness of each layer=0.8/4=0.2m

Therefore, Mass of each node = 6.3 m^2* 0.2 m* ρ (kg/m^3)

Where, ρ= Density of soil for Phoenix=1200 kg/m^3

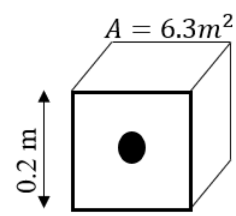

Figure 13 Volume of fictitious cuboid enclosing node

Mass appropriation is a crucial step in basement model as this cold mass protects basement from an otherwise torrid environment around the dwelling for a significant period. If the building is subjected to such extreme weather for a longer period, cooling capacity of soil decreases gradually resulting in zonal temperatures that actively follow change in outdoor temperature.

Hence, the lower temperature in basement may provide refuge to building occupants in the event of a hot spell with no mechanical cooling for some time.

Wall section 2 and 3 as well as floor of the basement is assumed to be connected to an adiabatic node. The temperature of this adiabatic node is calculated by running the model with TMY3 weather file for 10 years as a warm up to find ground temperatures.

2.5.2 Shading

As discussed in section 2.2.2 , Palo verde with fixed height is simulated for a "best shading" scenario. Also, section 2.3 discusses the way to calculate solar loads on nodes representing exposed surfaces. Loads calculated by the subroutine (solarincident.m) needs to be multiplied by a shading coefficient ($F_{shad,i}$) representative of tree in consideration.

Shade cast by a tree depends not only on its dimensions and opacity but also on time of day, date which determines the sun-path on that particular day. July 15th has been assumed for calculation of all shading coefficients.

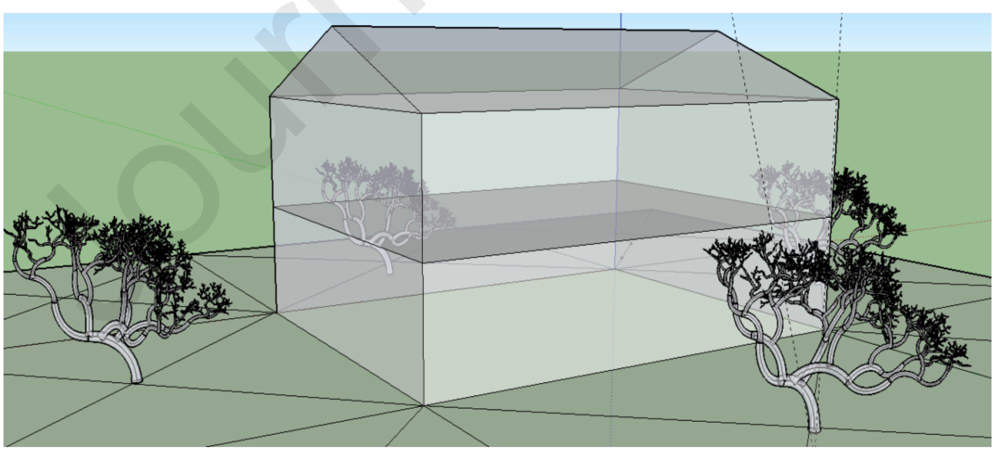

Figure 14 Shading analysis using SketchUp

Error! Reference source not found.3 illustrates the import of geometry of tree from the landscape tool of SketchUp around the house model obtained from PNNL prototypes. Trees are placed at a distance of 3 meters from the house facing all the walls, windows and partly shading the roof. 3D geometry of the whole system once assembled, is exported in .3ds format and subsequently imported in Autodesk Ecotect (legacy) tool. Surface Shading tool in the sun path wizard of Ecotect provides shading coefficients for chosen surface accurate up-to 2 decimal digits randomized (points) over the whole surface in the direction of surface normal vector.

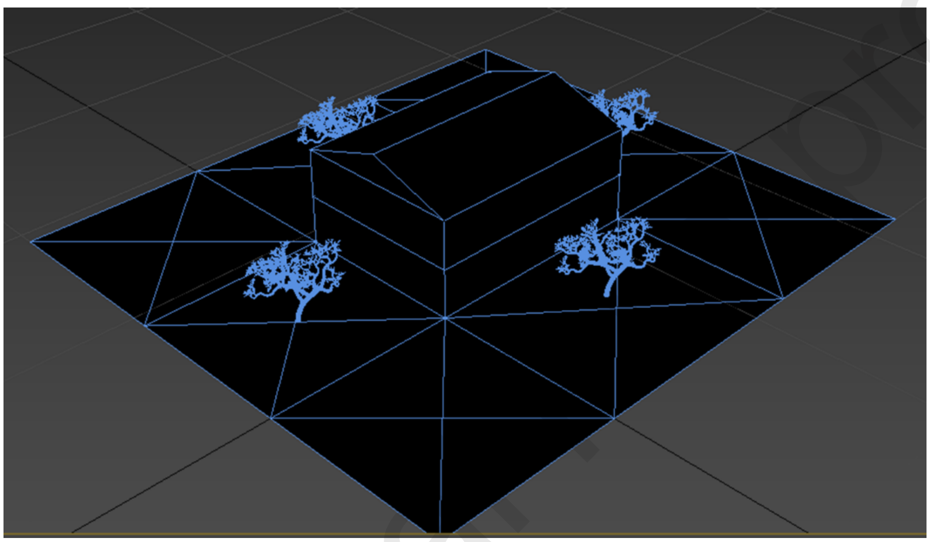

Figure 15 Export of tree and building geometry in Ecotect

This process is repeated for each direction and the results with shading coefficient for each hour of the day for each direction is obtained. (see **Error! Reference source not found.**4)

July 15th	1st FL, South	2nd FL, South	1st FL, West	2nd FL, West	1st FL, North	2nd FL, North	1st FL, East	2nd FL, East	Roof facing South	Roof facing West	Roof facing North	oof facing Ea
0	0	0	0	0	0	0	0	0	0	0	0	0
1	0	0	0	0	0	0	0	0	0	0	0	0
2	0	0	0	0	0	0	0	0	0	0	0	0
3	0	0	0	0	0	0	0	0	0	0	0	0
4	0	0	0	0	0	0	0	0	0	0	0	0
5	0	0	0	0	0.02	0	0.18	0.015	0.085	0	0.12	0
6	0	0	0	0	0	0	0.045	0	0.13	0	0.21	0.06
7	0	0	0	0	0.05	0.11	0.055	0.075	0.31	0	0.535	0
8	0.03	0.06	0	0	0.09	0.06	0.115	0.08	0.715	0	0.71	0.03
9	0.425	0.185	0	0	0	0	0.095	0.225	0.94	0	0.84	0.115
10	0.735	0.32	0	0	0	0	0.505	0.58	1	0	0.99	0.115
11	0.89	0.46	0	0	0	0	0.475	0.075	1	0	1	0.06
12	0.86	0.45	0.88	0.375	0	0	0	0	1	0.06	1	0
13	0.735	0.33	0.35	0.6	0	0	0	0	0.995	0.255	1	0
14	0.565	0.15	0.03	0.215	0	0	0	0	0.955	0.09	0.895	0
15	0	0.05	0.01	0.145	0.03	0.09	0	0	0.745	0.03	0.775	0
16	0	0	0.08	0.075	0.02	0.1	0	0	0.31	0.06	0.59	0
17	0	0	0.125	0.03	0.01	0	0	0	0.15	0	0.29	0
18	0	0	0.365	0.045	0.13	0	0	0	0.125	0	0.05	0
19	0	0	0	0	0	0	0	0	0	0	0	0
20	0	0	0	0	0	0	0	0	0	0	0	0
21	0	0	0	0	0	0	0	0	0	0	0	0
22	0	0	0	0	0	0	0	0	0	0	0	0
23	0	0	0	0	0	0	0	0	0	0	0	0

Figure 16 Shading coefficients for exposed surfaces

The values thus obtained are plugged in equation (3) to actualize revised solar loads.

2.5.3 Humidity Model

A humidity model is required in this exercise to ascertain relative humidity, dew point temperature and vapor pressure for indoor environment quality assessment and calculation of Heat Stress Indices to be presented in future publications. It is based on a macro moisture balance based on net influx of moisture by ventilation, internal production from human activity, and the net removal of moisture by the HVAC system if applicable:

$$\frac{\mathrm{dm_{w,sys}}}{\mathrm{dt}} = \sum \dot{\mathrm{m}}_{\mathrm{w,in}} - \sum \dot{\mathrm{m}}_{\mathrm{w,\,out}} + m_{gen} \qquad (3)$$

Where,

$\frac{dm_{w,sys}}{dt}$= Change in total amount of moisture in the room

$\sum \dot{\mathrm{m}}_{\mathrm{w,in}}$=mass flow rate of moisture (inflow) (kg/kg)

$\sum \dot{\mathrm{m}}_{\mathrm{w,out}}$=mass flow rate of moisture (outflow) (kg/kg)

m_{gen}= moisture generated through respiration of occupants (kg/hour)

Moisture generation: Moisture is generated inside the building by many sources such as cooking, washers and dryers, showers etc. However, since we are simulating a rare event in which power is lost for 5 days, schedule of moisture generation will depend whether the occupants have access to any appliances or water supply.

Therefore, moisture generation by use of appliances and showers has not been included. Moisture generation by occupants can be in the form of respiration or perspiration which would depend on the level of activity and environmental conditions of the room (like humidity and temperature). In this study, moisture generated by respiration is considered constant and equal to 0.5 kg/hour per person.

Moisture (Inflow): As discussed in section 2.2.3, ventilation and infiltration allow outdoor air to enter inside the building space, extent of which depends on the vintage of building and HVAC supply air design (keeping density of air constant). Corresponding proportional specific humidity obtained from WRF data is the inflow of moisture inside the building.

Section 2.2.4 gives an overview of HVAC (sensible cooling) sizing calculations. When an air conditioner is switched on, the supply air temperature is 18° C and specific humidity of the conditioned supply air is assumed to be 0.008 kg/kg. Moisture influx in a zone due to air conditioner may be calculated assuming an air change rate of 4 per hour (due to air conditioner) with given specific humidity.

Moisture (Outflow): To maintain the mass balance of the system, volume of air coming inside the room should be equal to volume of air going out of room (density being constant). However, the air going out of the room now contains added moisture from supply air of air conditioner as well as moisture generated by occupants. Moisture content of outgoing air is assumed equal to specific humidity in the room in previous time step (H^{-1}).

3 Heat transport mechanisms that determine the thermal behavior during a heat wave

The simulation duration is divided into three phases namely, pre-power outage, power outage and post power outage. Effect of boundary conditions on system (building envelope, HVAC design and moisture model) in these three phases would determine the response of dynamic building environment.

3.1 Phase 1: Pre-power outage

Phase 1 is the event in simulation timeline when control shifts from typical meteorological year weather to parcel data generated by WRF. As the vintage of residences gets old, even otherwise normal operation of adequately designed system may be insufficient to provide satisfactory comfort conditions due to increased infiltration and haggard HVAC in addition to obsolete building components like inefficient single pane highly conductive window glasses and frames. Thermal response of building in this phase determines the adaptability of occupants to higher than recommended comfortable temperatures which subsequently determines the severity of heat exposure in phase 2 of simulation timeline. This phenomenon will be studied in detail in future work and is beyond the scope of this paper.

3.2 Phase 2: Power outage and heat wave

During power outage, dwellings rely solely on passive cooling of house as mechanical mode of cooling are unavailable. Heat fluxes are driven by natural agents such as solar heat gain, ventilation dependent on wind speed (and occupant control), infiltration, radiative cooling at night and deep soil acting as heat sink for walls soaking heat from environment. Following section discusses importance of active mass and night cooling in impeding the sudden rise in indoor temperatures in this phase.

This accumulated heat (during the day) finds sink through two mechanisms;
Active Mass: The soil beneath building floor remains cool as it does not have solar radiation beaming on it. In residences where, conditioned spaces are positioned above slab on grade floor (without basement), soil beneath them are further cooled by the consistently cold conditioned temperatures (of thermal zone) due to mechanical cooling. These two factors along-with active mass of soil (storage) maintains a heat sink for the building which can absorb heat flux gained by rest of the building envelope and retard the rise in temperature inside the house.

Dwellings with below grade basement benefit from this damping property of soil by having a basement with relatively colder temperatures (no solar heat gain) as compared to other zones of the house (living room floor and bedroom floor of two story detached house with basement). When the air conditioner is ON, conditioned air also flows to the basement such that the air in the room is changed every hour, bringing in air flow from the AC.

Night cooling: Radiative exchange in the night is particularly effective for climates with large diurnal swings and minimal cloud cover as in the case of Phoenix. Sky temperature is computed by the longwave radiation data of WRF. The radiative exchange between built form and sky in the night is significant as sky temperatures are lower than the ambient temperature and the hot walls and roof of building are able to radiate back some of the heat. The amount of heat flux depends on area of walls and their emissivity. Emissivity being constant (wall construction property), buildings with larger skin to volume ratio such as detached houses will lose heat rapidly as compared to apartments that are a small part of the larger built mass.

On the flip side, large skin to volume ratio may also result in higher heat absorption during the day with typical wall absorptivity as high as 0.8.

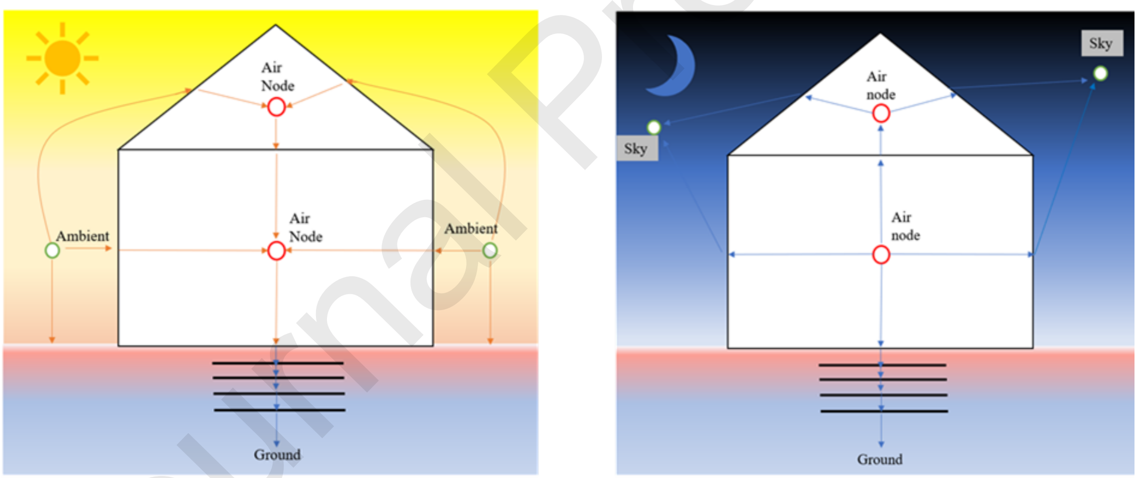

(a) (b)

Figure 17 Heat sink mechanisms for buildings (a) Ground heat transfer (b) Radiative night cooling

3.3 Phase 3: Post-power outage

After restoration of electricity, HVAC system starts to operate at the capacity that it was operating in the pre-outage period. However, since the buildings are exposed to intense heat for a length of time, the building mass soaks a substantial amount of heat despite mechanisms decelerating heat gain, as discussed in the previous section. For buildings which are deprived of these architectural advantages, the recovery period might be longer than other prototypes. For instance, an apartment facing North direction and surrounded by other apartments on all sides benefit only from ground active mass as its skin to volume ratio is lesser than other building archetypes. On the other hand, apartment on the South-East corner of a multi-story building has comparatively larger skin to volume ratio but is not directly linked to ground, isolating it from cool active mass.

3.4 Reported Outcomes

A colossal amount of data generated after running the batch simulations needed a structure for its representation. Three separate batches were run with HVAC efficiency 100%, 50% and 0% and packaged in 3 dimensional matrices saved as .mat files. Figure 18 shows data framework for one batch run.

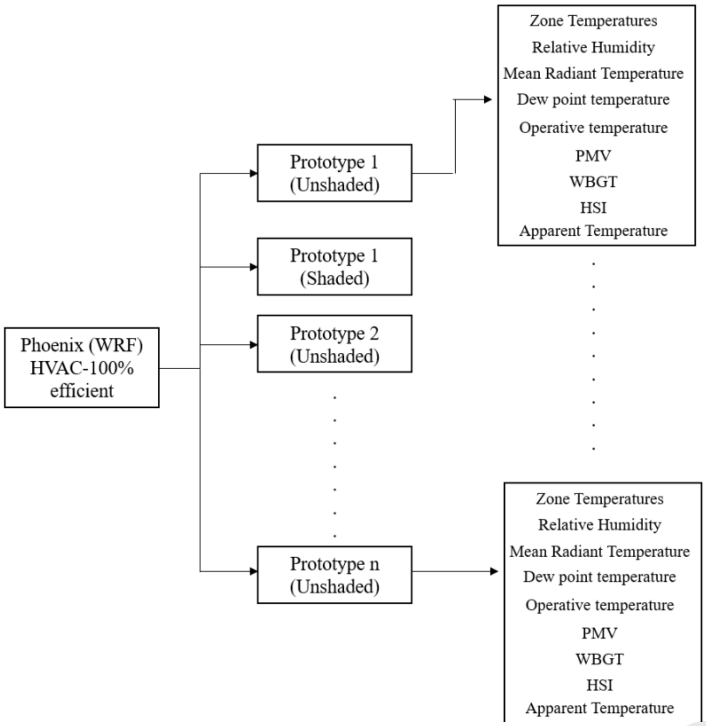

Figure 18 Data structure for one batch run

Each .mat file has dimensions 222 (IEQ parameters) x528 (hours) x1800 (grids).

4 Results and Discussion

Due to large number of prototypes and zones in them, each thermal zone has been numbered to represent the part of house that is covered by it. **Error! Reference source not found.** Shows the prototypes and their zones for reference in results.

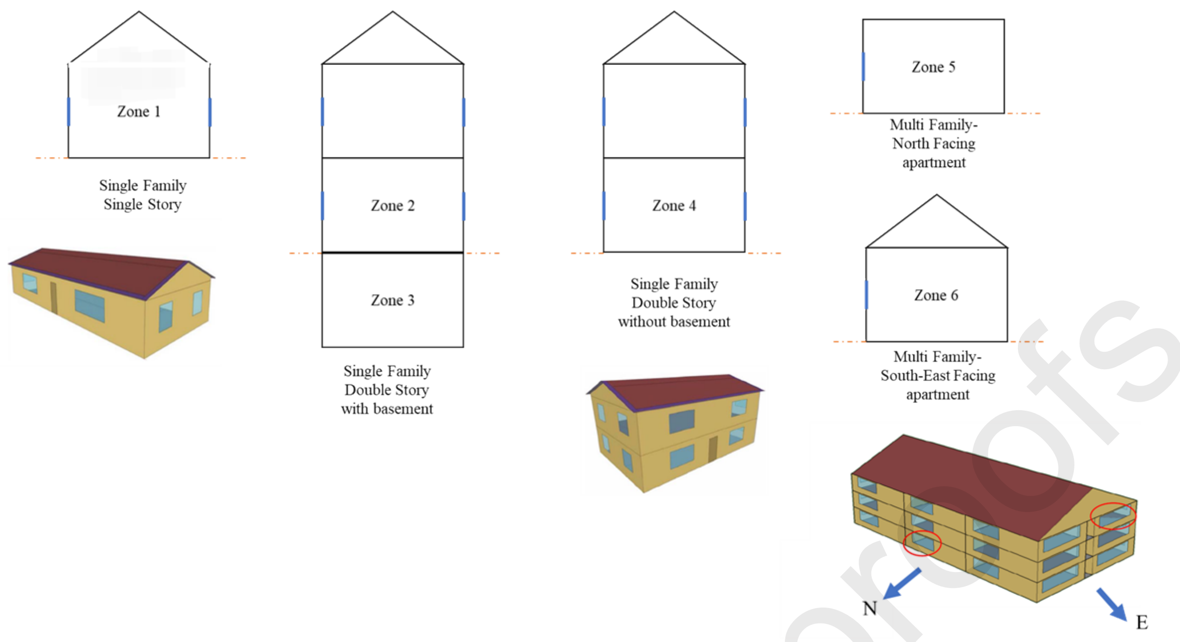

Figure 19 Thermal zones in building prototypes

In order to make it convenient for readers to comprehend the graphs, color scheme for zones are kept same in all the result figures. A representative grid no 542 (having highest temperature amongst all the grids) has been selected to represent thermal response of building prototypes and the effects of their variants in the microscopic view.

Table 5. Zone nomenclature

Zone	**House type**	**Acronym**
1(Living Room)	Single Family Single Story	SF
2 (Living Room), 3 (Basement)	Single Family Two story with basement	SFWB, Base
4 (Living Room)	Single family two story without basement	SFWOB
5 (Living Room)	Multi Family- North apartment	MS_N
6 (Living Room)	Multi family SE apartment	MS_SE

4.1 Variability across prototypes and their variants during power outage- A microscopic view

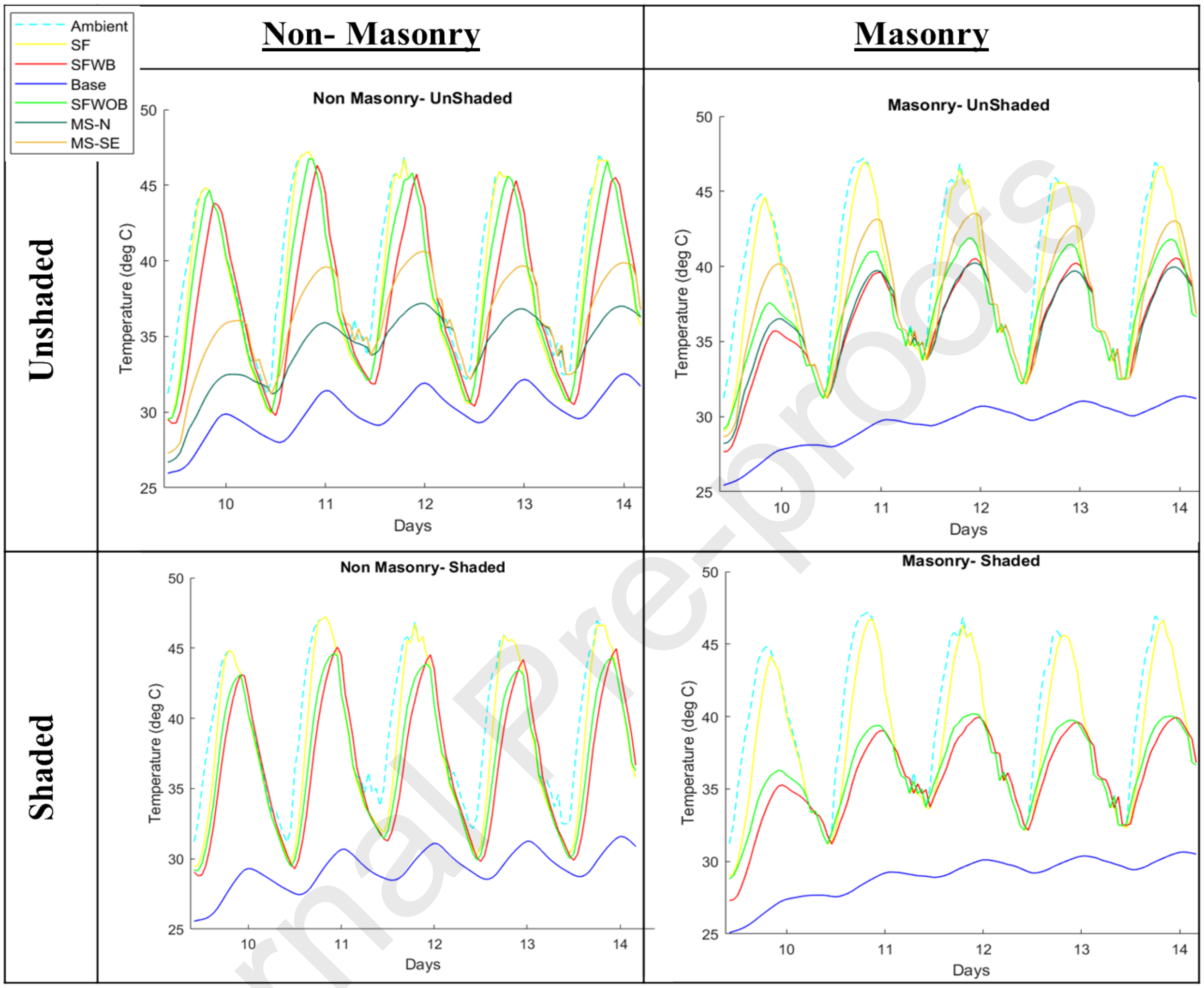

Figure 20 Temperature profiles in building prototypes

Figure 20 shows the temperature profiles of different zones in prototypes with variations of construction and shading for each of them in the hottest grid of the city.

4.1.1 Comparison of coldest zone in each prototype (including basement)

It may be observed from the figure that multi-family apartments and basements are the coolest areas amongst all zones considered due to the availability of residual cooling from active thermal mass in the event of a power outage. The basement, in addition to active mass, gets maximum shield from the high solar ingress as compared to other zones in consideration, making it the best location to seek refuge from high temperatures. Similarly, North facing ground floor apartments have relatively lower solar heat load and high active mass that resists the increase in temperature. Finally, temperature profiles of South-East facing apartments lie in between those of distinctly cooler zones and very high temperature zones such as living spaces of detached houses.

The living spaces of detached houses have comparable temperature profiles due to the presence of large windows that allow solar radiation to enter and stay in the space. Once, the temperature inside the built space overshoots the ambient temperature due to greenhouse effect of glass, windows are operated with an opening factor of 1. Opening of large windows on all four directions brings the inside air temperature close to the ambient temperature.

4.1.2 Comparison of masonry with non-masonry houses for mid century and end of century- need to phase out old houses?

The discussion on heat response of structures made of “Masonry vs Non-masonry” and “Shaded vs Non-shaded” constructions has relevance only for detached single family houses as prototypes of Multi-family apartments are compliant to different IECC requirements with steel frames without any assumption of immediate shading.

It should also be noted that Single family single story houses are modeled as structures that do not have attic insulation to highlight its importance in thermal performance of residential dwellings. The absence of attic insulation in Zone 1 shows that the temperature profile between masonry and non-masonry structures is almost identical highlighting the fact that solar load from the roof takes the temperature to a point where windows are operated and indoor air temperature follows ambient temperatures.

On the other hand, masonry structures with attic insulation show that with high active mass of bricks along-with insulation resist the increase in the air temperature inside the house with a difference of up-to 4°C as compared to the non-masonry counterparts. The temperature of basement shows remarkably low diurnal swings in temperature. These findings suggest the use of traditional knowledge of high mass constructions such as Adobe houses with contemporary insulation technologies can maximize the energy efficiency as well as resilience of residential structures.

The effect of shading, though minimal, can also be seen when the living space is insulated from solar loads of roofs. The effect of shading is subdued due to the assumption of less dense, xerophobic trees for landscape design that block a very small amount of solar radiation falling on the facades.

4.2 Variability across city

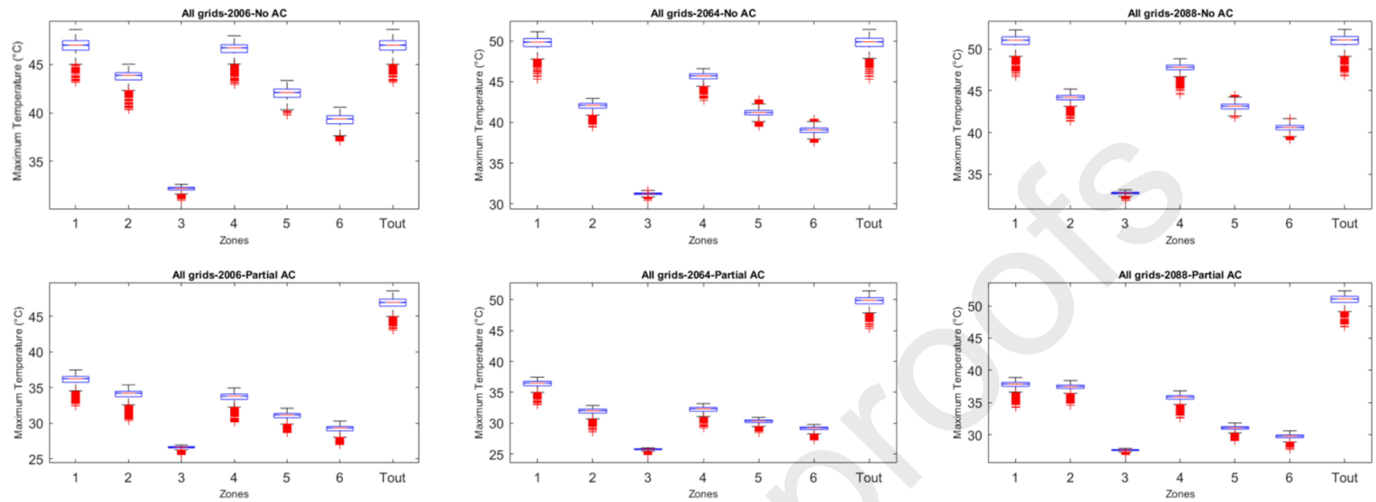

Figure 21 Variation of Ambient and prototype temperatures across city grids

Figure 21 shows the variability in indoor temperatures across all grids at the peak of heat wave, i.e., at the time of maximum outdoor temperature. The ambient temperature at that hour is represented as a box plot (T_{out}) taking data from all grids of the city. The figure shows two scenarios, namely:

- Having no cooling potential during the power outage
- Having partial cooling capacity during the power outage

Partial cooling scenario represents the deficient HVAC systems that exist in dilapidated ill maintained structures. This result aims to highlight the exposure of residents in lower strata of the society, where, adequate cooling is not available even in routine building operations.

The jump in heat exposure from adequate cooling (during routine operations) to no cooling (during heatwave) is variable depending on the rise in temperature in mid-century and end of century scenarios ranging from 10°C at start of the century to a startling 15°C in 2088, assuming a setpoint of 24°C. These results highlight the grim reality of thermal comfort in low income houses across the globe where unavailability of air conditioning during extreme weather exacerbates the pre-existing heat sensitive medical conditions such as diabetes, heart diseases and asthma resulting in much higher morbidity as compared to affluent neighborhoods that can afford better living conditions owing to superior building envelopes and air conditioning equipment.

It is also interesting to note that if only partial cooling is available due to decentralized power generation such as solar rooftop PV or batteries, the exposure relative to setpoint can be decreased from a delta of 23°C to 11°C, which is a significant when we consider the correlation between temperature and mortality during a heat wave (see Figure 22).

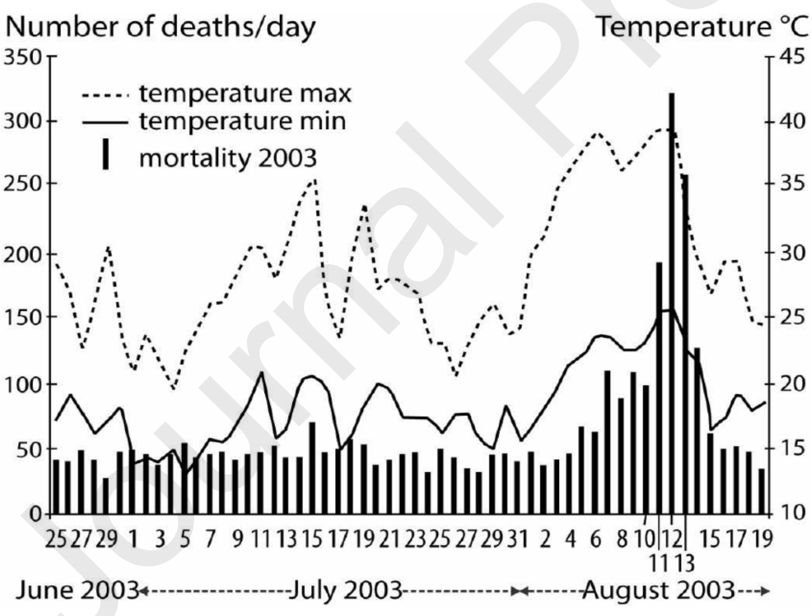

Figure 22 Number of deaths at varying temperatures during Paris heatwave (Dousset et al., 2010)

It is also noteworthy that there is a high degree of variability in ambient temperature across different grids in the city with a range of up to 5°C, again, making some neighborhoods of the city more vulnerable to health effects of heat stress.

From the perspective of building science, single story detached houses exhibit the highest heat exposures as compared to 2-story detached housed due to insulation from heat gained through roof. Furthermore, the presence of a basement supplies a small amount of cooling to the living spaces of these houses. Basement and multi-family zones have the least heat exposure for its occupants.

4.3 Effectivity of mitigation strategies

Building models that represent building stock of Phoenix were tested for current and future weather scenarios with extreme mitigation measures such as a blanket adoption of cool roofs and extensive tree planting drive across the city. Figure 23 and table 6 shows the maximum indoor temperature during heat wave for a single prototype of single family two story house without basement across all grids of the city. The red text in table highlights the reduction in temperature as compared to no adaptation scenario in the same column.

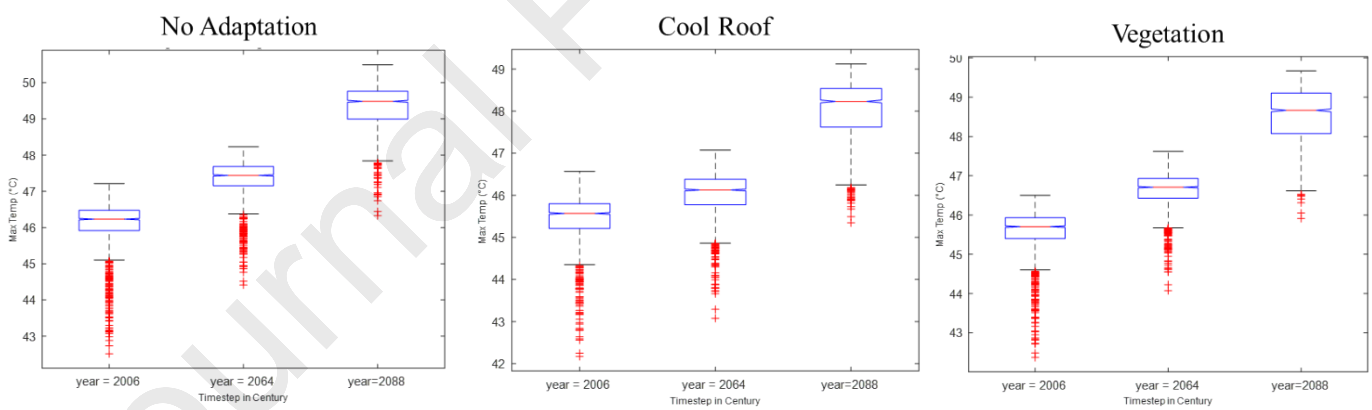

Figure 23 Highest temperature in all grids for different mitigation scenarios

Some interesting observations can be made from the descriptive statistics of maximum temperature in all grid cells;

- The number of outliers on the lower end of the distribution keeps diminishing as the century progresses indicating that as urbanization increases, grids that once had relatively lower urban heat island effect would become warmer due to change in land use.

Table 6 Difference in temperatures due to urban mitigation strategies

	2006			2064			2088		
	Mean	Max	Min	Mean	Max	Min	Mean	Max	Min
No Adaptation	46.23	47.21	42.51	47.44	48.22	44.41	49.45	50.5	46.33
Cool Roof	45.56 /0.67	46.57 /0.64	42.17 /0.34	46.10 /1.34	47.07 /1.15	43.08 /1.33	48.23 /1.22	49.12 /1.38	45.35 /0.98
Vegetation	45.68 /0.55	46.5/ 0.71	42.36 /0.15	46.68 /0.76	47.62 /0.6	44.07 /0.34	48.62 /0.83	49.66 /0.84	45.91 /0.42

- The mitigation in extreme temperatures of hottest grid is almost twice that of coldest grid in both mitigation scenarios. The hottest grids benefit more from these mitigation strategies as they are more affected by the urban heat island effect.
- Cool roofs prove to be a better strategy if only temperature reduction is the only metric for decision makers.

5 Conclusions

We have analyzed the heat response of different kind of buildings and their variants in the event of heat waves that are influenced by climate change over the span of a century. In the absence of adequate cooling due to deficient HVAC and/or power outages, the heat exposure of these structures is very high and the city needs adaptation strategies to diminish the harmful impact on health of its residents in such an event.

Basements and multi-family apartments remain the places where the impact of heat waves is slightly toned down. These zones become quite resilient if they are constructed with high active mass and sufficient insulation on the interior of the living space. However, basements have been rather uncommon in Phoenix due to high costs attached with it.

Other means of tapping the cooling from active thermal mass beneath the house can be by building slightly below grade living spaces in addition to high thermal mass in the South direction and overhangs on windows that receive high solar insolation.

Adaptation strategies such as installation of battery-operated cooling devices and on-site renewable energy generation for evaporative cooling may also alleviate the heat stress from very high temperatures.

Lastly, there is a high variability of up to 5°C in ambient conditions across the city in every timeframe considered in this study, evincing the inequality that residents face in terms of both, economic burden due to energy bills as well as overheating in unfavorable circumstances. Targeted push by city authorities for above discussed mitigation and adaptation strategies can achieve energy and social equality in impoverished areas of the city.

This paper represents a fraction of otherwise large study which aims to quantify the impact of rare concurrent events of power outage during a heat wave in three cities of Phoenix, Detroit and Atlanta. Thereafter, adaptation strategies of increasing albedo using cool roofs and expanding vegetation cover in the three cities is simulated. Follow up papers would include heat exposure results from Atlanta and Detroit along-with measures that capture the heat stress of occupants, based on simulated indoor environment. Among those used are well established thermal comfort measures such as operative temperature, Fanger's predicted mean vote and Wet Bulb Globe Temperature. The authors hope that this study would contribute to the discussion of resiliency in built spaces and help cities in formulating their adaptation strategies.

Acknowledgements

This material is based upon work supported by the National Science Foundation under Grant Number 1520803. Any opinions, findings, and conclusions or recommendations expressed in this material are those of the author(s) and do not necessarily reflect the views of the National Science Foundation.

Declaration of Competing Interest

The authors declare that they have no known competing financial interests or personal relationships that could have appeared to influence the work reported in this paper.

References

2017 ASHRAE® Handbook - Fundamentals (SI Edition). (2017). American Society of Heating Refrigerating and Air-Conditioning Engineers Inc.

Adkins, R. (n.d.). A guide to trees in Phoenix. (City of Phoenix) Retrieved from https://www.phoenix.gov/parks/parks/urban-forest/a-guide-to-trees-in-phoenix

Akbari, H., Kurn, D. M., Bretz, S. E., & Hanford, J. W. (1997). Peak power and cooling energy savings of shade trees. *Energy and Buildings*, *25*(2), 139–148. https://doi.org/10.1016/S0378-7788(96)01003-1

2017 ASHRAE® Handbook - Fundamentals (SI Edition). (2017). American Society of Heating Refrigerating and Air-Conditioning Engineers Inc.

Akbari, H. (2009). Cooling our communities. A guidebook on tree planting and light-colored surfacing.

Anderson, G. B., & Bell, M. L. (2012). Lights out: Impact of the August 2003 power outage on mortality in New York, NY. *Epidemiology*, *23*(2), 189–193. https://doi.org/10.1097/EDE.0b013e318245c61c

Augenbroe, G., Brown, J., Heo, Y., Kim, S. H., Li, Z., McManus, S., & Zhao, F. (2008). LESSONS FROM AN ADVANCED BUILDING SIMULATION COURSE. *Proceedings of SimBuild*, *3*(1), 261–268. Retrieved from http://www.ibpsa-usa.org/index.php/ibpusa/article/view/262

Baniassadi, A., Heusinger, J., & Sailor, D. J. (2018). Energy efficiency vs resiliency to extreme heat and power outages: The role of evolving building energy codes. *Building and Environment*, *139*, 86–94. https://doi.org/10.1016/j.buildenv.2018.05.024

Beniston, M. (2004). The 2003 heat wave in Europe: A shape of things to come? An analysis based on Swiss climatological data and model simulations. *Geophysical Research Letters*, *31*(2). https://doi.org/10.1029/2003GL018857

Berry, C (2015). *Residential Energy Consumption Survey 2015* U.S Energy Information Administration *https://www.eia.gov/consumption/residential/reports/2015/energybills/*

Bierwagen, B. G., Theobald, D. M., Pyke, C. R., Choate, A., Groth, P., Thomas, J. V., & Morefield, P. (2010). National housing and impervious surface scenarios for integrated climate impact assessments. *Proceedings of the National Academy of Sciences of the United States of America*, *107*(49), 20887–20892. https://doi.org/10.1073/pnas.1002096107

Broadbent, A. M., Krayenhoff, E. S., & Georgescu, M. (2020). Efficacy of cool roofs at reducing pedestrian-level air temperature during projected 21st century heatwaves in Atlanta, Detroit, and Phoenix (USA). *Environmental Research Letters*, *15*(8), 084007. https://doi.org/10.1088/1748-9326/ab6a23

Bruse, M. (2004). *ENVI-met 3.0: Updated Model Overview*. Retrieved from www.envi-met.com

Bueno, B., Norford, L., Hidalgo, J., & Pigeon, G. (2013). The urban weather generator. *Journal of Building Performance Simulation*, *6*(4), 269–281. https://doi.org/10.1080/19401493.2012.718797

Chan, W. R., Nazaroff, W. W., Price, P. N., Sohn, M. D., & Gadgil, A. J. (2005). Analyzing a database of residential air leakage in the United States. *Atmospheric Environment*, *39*(19), 3445-3455.

Ciancio, V., Falasca, S., Golasi, I., Curci, G., Coppi, M., & Salata, F. (2018). Influence of input climatic data on simulations of annual energy needs of a building: Energyplus and WRF modeling for a case study in Rome (Italy). *Energies*, *11*(10), 2835. https://doi.org/10.3390/en11102835

Cort, K. A., & Butner, R. S. (2012). *An Analysis of Statewide Adoption Rates of Building Energy Code by Local Jurisdictions*. https://doi.org/10.2172/1076722

Djongyang, N., Tchinda, R., & Njomo, D. (2010). Thermal comfort: A review paper. *Renewable and Sustainable Energy Reviews*, *14*(9), 2626–2640. https://doi.org/10.1016/J.RSER.2010.07.040

Dousset, B., Gourmelon, F., Laaidi, K., Zeghnoun, A., Giraudet, E., Bretin, P., Mauri, E.,Vandentorren, S. (2010). Satellite monitoring of summer heat waves in the Paris metropolitan area. International Journal of Climatology, 31(2), 313–323.http://doi.org/10.1002/joc.2222

Hamdy, M., Carlucci, S., Hoes, P. J., & Hensen, J. L. (2017). The impact of climate change on the overheating risk in dwellings—A Dutch case study. *Building and Environment*, *122*, 307-323.

Falasca, S., Ciancio, V., Salata, F., Golasi, I., Rosso, F., & Curci, G. (2019). High albedo materials to counteract heat waves in cities: An assessment of meteorology, buildings energy needs and pedestrian thermal comfort. *Building and Environment*, *163*, 106242. https://doi.org/10.1016/j.buildenv.2019.106242

Fouillet, A., Rey, G., Laurent, F., Pavillon, G., Bellec, S., Guihenneuc-Jouyaux, C., … Hémon, D. (2006). Excess mortality related to the August 2003 heat wave in France. *International Archives of Occupational and Environmental Health*, *80*(1), 16–24. https://doi.org/10.1007/s00420-006-0089-4

Hwang, W. H., Wiseman, P. E., & Thomas, V. A. (2015). Tree planting configuration influences shade on residential structures in four US cities. *Arboriculture & Urban Forestry*, *41*(4), 208–222.

Huang, K., Lee, X., Stone Jr, B., Knievel, J., Bell, M. L., & Seto, K. C. (2021). Persistent increases in nighttime heat stress from urban expansion despite heat island mitigation. *Journal of Geophysical Research: Atmospheres*, *126*(4), e2020JD033831.

Jeong, B., Jeong, J.-W., & Park, J. S. (2016). Occupant behavior regarding the manual control of windows in residential buildings. *Energy and Buildings*, *127*, 206–216. https://doi.org/10.1016/J.ENBUILD.2016.05.097

Kolokotroni, M., Ren, X., Davies, M., & Mavrogianni, A. (2012). London's urban heat island: Impact on current and future energy consumption in office buildings. *Energy and Buildings*, *47*, 302–311. https://doi.org/10.1016/J.ENBUILD.2011.12.019

Krayenhoff, E. S., Christen, A., Martilli, A., & Oke, T. R. (2014). A multi-layer radiation model for urban neighbourhoods with trees. *Boundary-layer meteorology*, *151*(1), 139-178.

Krayenhoff, E. S., Moustaoui, M., Broadbent, A. M., Gupta, V., & Georgescu, M. (2018). Diurnal interaction between urban expansion, climate change and adaptation in US cities. *Nature Climate Change*, *8*(12), 1097–1103. https://doi.org/10.1038/s41558-018-0320-9

Lee, S. J., Parrott, K. R., & Ahn, M. Exploring Housing Conditions of Low-Income Minorities in the Southern United States.

Lim, H., & Zhai, Z. J. (2017). Review on stochastic modeling methods for building stock energy prediction. *Building Simulation*, *10*(5), 607–624. https://doi.org/10.1007/s12273-017-0383-y

Liu, S., Pan, W., Zhang, H., Cheng, X., Long, Z., & Chen, Q. (2017). CFD simulations of wind distribution in an urban community with a full-scale geometrical model. *Building and Environment*, *117*, 11–23. https://doi.org/10.1016/J.BUILDENV.2017.02.021

Lomas, K. J., & Porritt, S. M. (2017a). Overheating in buildings: lessons from research. *Building Research & Information*, *45*(1–2), 1–18. https://doi.org/10.1080/09613218.2017.1256136

Lomas, K. J., & Porritt, S. M. (2017b, February 17). Overheating in buildings: lessons from research. *Building Research and Information*, Vol. 45, pp. 1–18. https://doi.org/10.1080/09613218.2017.1256136

Luber, G., & McGeehin, M. (2008). Climate Change and Extreme Heat Events. *American Journal of Preventive Medicine*, *35*(5), 429–435. https://doi.org/10.1016/J.AMEPRE.2008.08.021

Mallen, E. S. (2019). *A methodological assessment of extreme heat mortality modeling and heat vulnerability mapping in Atlanta, Detroit, and Phoenix* (Doctoral dissertation, Georgia

Institute of Technology).

Martilli, A., Clappier, A., & Rotach, M. W. (2002). An urban surface exchange parameterisation for mesoscale models. *Boundary-Layer Meteorology*, *104*(2), 261–304. https://doi.org/10.1023/A:1016099921195

Masson, V., Grimmond, C. S. B., & Oke, T. R. (2002). Evaluation of the Town Energy Balance (TEB) Scheme with Direct Measurements from Dry Districts in Two Cities, *Journal of Applied Meteorology*, *41*(10), 1011-1026.

McGeehin, M. A., & Mirabelli, M. (2001). The Potential Impacts of Climate Variability and Change on Temperature-Related Morbidity and Mortality in the United States. *Environmental Health Perspectives*, *109*, 185. https://doi.org/10.2307/3435008

McPherson, E. G., & Dougherty, E. (1989). Selecting trees for shade in the Southwest. *Journal of Arboriculture*, *15*(2), 35–43.

Monitored in-situ performance of residential air-conditioning systems / Discussion - ProQuest. (n.d.). Retrieved May 28, 2021, from https://www.proquest.com/docview/192579263?pq-origsite=gscholar&fromopenview=true

Rebetez, M., Dupont, O., & Giroud, M. (2009). An analysis of the July 2006 heatwave extent in Europe compared to the record year of 2003. *Theoretical and Applied Climatology*, *95*(1–2), 1–7. https://doi.org/10.1007/s00704-007-0370-9

Simpson, J. R. (2002). Improved estimates of tree-shade effects on residential energy use. *Energy and Buildings*, *34*(10), 1067–1076. https://doi.org/10.1016/S0378-7788(02)00028-2

Skamarock, W. C., Klemp, J. B., Dudhia, J., Gill, D. O., Barker, D. M., Wang, W., & Powers, J. G. (2005). *A description of the advanced research WRF version 2*. National Center For Atmospheric Research Boulder Co Mesoscale and Microscale Meteorology Div.

Stone, B., Mallen, E., Rajput, M., Broadbent, A., Krayenhoff, E. S., Augenbroe, G., & Georgescu, M. (2021). Climate change and infrastructure risk: Indoor heat exposure during a concurrent heat wave and blackout event in Phoenix, Arizona. *Urban Climate*, *36*. https://doi.org/10.1016/j.uclim.2021.100787

Touchaei, A. G., & Akbari, H. (2015). Evaluation of the seasonal effect of increasing albedo on urban climate and energy consumption of buildings in Montreal. *Urban Climate*, *14*, 278–289. https://doi.org/10.1016/j.uclim.2015.09.007

Vellei, M., Ramallo-González, A. P., Coley, D., Lee, J., Gabe-Thomas, E., Lovett, T., & Natarajan, S. (2017). Overheating in vulnerable and non-vulnerable households. *Building Research & Information*, *45*(1–2), 102–118. https://doi.org/10.1080/09613218.2016.1222190

Wang, Z.-H., Zhao, X., Yang, J., & Song, J. (2016). Cooling and energy saving potentials of shade trees and urban lawns in a desert city. *Applied Energy*, *161*, 437–444. https://doi.org/10.1016/j.apenergy.2015.10.047

Zhao, F., Lee, S. H., & Augenbroe, G. (2016). Reconstructing building stock to replicate energy consumption data. *Energy and Buildings*, *117*, 301–312.

https://doi.org/10.1016/j.enbuild.2015.10.001

Appendix

Table 7 Units for all construction details

Units	
Thickness	Metre
Rho	kg/m3
Conductivity	W/m-K
Specific Heat Capacity	J/kg-K
U-factor	W/m2-K
SHGC	Dimensionless

Table 8 Masonry Construction

Exterior Wall				
	Thickness	rho	specific heat capacity	conductivity
Stucco	0.025	1922	878.6	0.6918
Polystyrene	0.0506	24	1300	0.0206
Concrete Block	0.15	1920	800	0.8648
OSB 5/8"	0.012	544.6	1213	0.8648
Exterior Roof				
	Thickness	rho	specific heat capacity	conductivity
Asphalt Shingle	0.0063	1121	1255	0.081
OSB 0.5"	0.012	544.6	1213.3	0.1163
Exterior Floor				
	Thickness	rho	specific heat capacity	conductivity
Carpet & Pad	0.025	32	836	0.06
Plywood 3/4"	0.019	544	674	0.1154
Floor Console	0.05	55.07	916	0.048
Soil	0.8	1200	1100	0.7
Window				
	Thickness	rho	specific heat capacity	U-factor
Glass	0.01	2400	1200	5.8
	SHGC			
	0.7			
Interior Ceiling				
	Thickness	rho	specific heat capacity	conductivity
Cellulose Insulation	0.14	85	1800	0.04
Lumber	0.1	700	2090	0.21
Drywall 0.5"	0.0127	801	1087	0.16
Interior Floor				
	Thickness	rho	specific heat capacity	conductivity
Carpet & Pad	0.025	32	836	0.06
Plywood 3/4"	0.019	544	674	0.1154
Basement Wall				
	Thickness	rho	specific heat capacity	conductivity
Plywood 3/4"	0.019	544	674	0.1154

Basement console layer	0.000254	120.801	1036	0.06
Plywood 3/4"	0.019	544	674	0.1154

Table 9 Construction details ; IECC 2006

Exterior Wall				
	Thickness	rho	specific heat capacity	conductivity
Stucco	0.025	1922	878.6	1.39
Sheathing	0.012	685	1172	0.094
OSB 5/8"	0.0158	544.6	1213	0.1163
Wall console	0.021	120	1036.25	0.059
Dry Wall	0.012	800	1087	0.16
Exterior Roof				
	Thickness	rho	specific heat capacity	conductivity
Asphalt Shingle	0.0063	1121	1255	0.081
OSB 0.5"	0.012	544.6	1213.3	0.1163
Exterior Floor				
	Thickness	rho	specific heat capacity	conductivity
Carpet & Pad	0.025	32	836	0.06
Plywood 3/4"	0.019	544	674	0.1154
Floor Console	0.05	55.07	916	0.048
Soil	0.8	1200	1100	0.7
Window				
	Thickness	rho	specific heat capacity	U-factor
Glass	0.01	2400	1200	4.2585
	SHGC			
	0.4			
Interior Ceiling				
	Thickness	rho	specific heat capacity	conductivity
Ceiling console layer	0.21	41.92	776	0.04
Drywall 0.5"	0.0127	801	1087	0.16
Interior Floor				
	Thickness	rho	specific heat capacity	conductivity
Carpet & Pad	0.025	32	836	0.06
Plywood 3/4"	0.019	544	674	0.1154
Basement Wall				
	Thickness	rho	specific heat capacity	conductivity
Plywood 3/4"	0.019	544	674	0.1154
Basement console layer	0.000254	120.801	1036	0.06
Plywood 3/4"	0.019	544	674	0.1154

Table 10 Construction details; IECC 2012

Exterior Wall				
	Thickness	rho	specific heat capacity	conductivity
Stucco	0.025	1922	878.6	1.39
Sheathing	0.012	685	1172	0.094
OSB 5/8"	0.0158	544.6	1213	0.1163
Wall console	0.021	120	1036.25	0.059
Dry Wall	0.012	800	1087	0.16
Exterior Roof				
	Thickness	rho	specific heat capacity	conductivity
Asphalt Shingle	0.0063	1121	1255	0.081
OSB 0.5"	0.012	544.6	1213.3	0.1163
Exterior Floor				
	Thickness	rho	specific heat capacity	conductivity
Carpet & Pad	0.025	32	836	0.06
Plywood 3/4"	0.019	544	674	0.1154
Floor Console	0.05	55.07	916	0.048
Soil	0.8	1200	1100	0.7
Window				
	Thickness	rho	specific heat capacity	U-factor
Glass	0.01	2400	1200	2.227
	SHGC			
	0.25			
Interior Ceiling				
	Thickness	rho	specific heat capacity	conductivity
Ceiling console layer	0.21	41.92	776	0.04
Drywall 0.5"	0.0127	801	1087	0.16
Interior Floor				
	Thickness	rho	specific heat capacity	conductivity
Carpet & Pad	0.025	32	836	0.06
Plywood 3/4"	0.019	544	674	0.1154